MASARYKOVA UNIVERZITA
Přírodovědecká fakulta
Ústav teoretické fyziky a astrofyziky

Diplomová práce

Brno 2016   Jakub Vulgan

MASARYKOVA UNIVERZITA
PŘÍRODOVĚDECKÁ FAKULTA
Ústav teoretické fyziky a astrofyziky

Slupkové galaxie - hydrodynamické simulace typu "sticky-particles"

Diplomová práce

Jakub Vulgan

Bibliographic Entry

Bibliografický záznam

Autor: Jakub Vulgan
Přírodovědecká fakulta, Masarykova univerzita
Ústav teoretické fyziky a astrofyziky

Název práce: Slupkové galaxie - hydrodynamické simulace typu "sticky-particles"

Studijní program: Fyzika

Studijní obor: Teoretická fyzika a astrofyzika

Vedoucí práce: RNDr. Bruno Jungwiert, Ph.D.

Akademický rok: 2015/16

Počet stran: xvi + 43

Klíčová slova: slupkové galaxie; Plummerův profil; Hernquistův profil; simulace; sticky-particles hydrodynamika

Abstract

In this thesis we carry out several numerical simulations that try to give birth to shells around galaxies through radial encounters of galaxies with high mass ratio (minor mergers). We use two theoretical gravity models - Plummer and Hernquist sphere. Simulations are carried out for stellar and gaseous shells with use of the "sticky-particles" hydrodynamics. Our goal is to compare properties of gaseous and stellar shells as well as describe differences between both gravitational profiles. We find out that the positions, intensities and angular widths of the shells differ significantly for chosen profiles and that the influence of hydrodynamics is not very big for typical ratios of gas in galaxies today.

Abstrakt

V této práci provádíme řadu numerických simulací, které se snaží za pomoci radiálních srážek galaxií s vysokým hmotnostním poměrem (tzv. minor merger) dat za vznik slupkám kolem galaxií. Využíváme dvou teoretických gravitačních profilů - Plummerovu a Hernquistovu sféru. Simulace provádíme pro hvězdné i plynné slupky za pomoci hydrodynamické metody "sticky-particles". Snažíme se porovnat vlastnosti plynných a hvězdných slupek a taktéž popsat rozdíly mezi oběma gravitačními profily. Zjišťujeme, že polohy, intenzity a uhly rozevření slupek jsou velmi odlišné pro námi zkoumané profily a že vliv hydrodynamiky je jen velmi malý pro dnes typické poměry plynu v galaxiích.

Masarykova univerzita

Přírodovědecká fakulta

ZADÁNÍ DIPLOMOVÉ PRÁCE

Student	: **Bc. Jakub Vulgan, učo <u>376108</u>**
Studijní program	: **Fyzika**
Studijní obor	: **Teoretická fyzika a astrofyzika**

Ředitel Ústavu teoretické fyziky a astrofyziky PřF MU Vám ve smyslu Studijního a zkušebního řádu MU určuje diplomovou práci s tématem:

<u>Slupkové galaxie - hydrodynamické simulace typu "sticky-particles"</u>

Shell galaxies - simulations with "sticky-particles" hydrodynamics

Zásady pro vypracování: Slupkové galaxie (shell galaxies) jsou charakterizovány přítomností ostře ohraničených obloukových útvarů (slupek) o poloměrech jednotek až stovek kiloparseků. Slupky vznikají v důsledku destruktivních srážek galaxií (tzv. mergery) a obvykle jsou tvořeny hvězdami, v některých případech jsou však pozorovány i v plynu. Cílem práce je simulace vzniku/vývoje slupkové struktury ve hvězdné i plynné složce zároveň a porovnání poloh, geometrie a tvaru spektrálních čar slupek v obou složkách. K modelování hydrodynamiky plynu bude použita metoda tzv. sticky-particles.

Jazyk závěrečné práce	: český, anglický nebo slovenský
Vedoucí diplomové práce	: RNDr. Bruno Jungwiert, Ph.D.
Datum zadání diplomové práce	: leden 2014
Datum odevzdání diplomové práce	: dle harmonogramu ak. roku 2014/2015

V Brně   leden 2014

Rikard von Unge

ředitel ÚTFA

Zadání diplomové práce převzal dne:

Podpis studenta

Poděkování

Ze všeho nejvíc bych chtěl poděkovat svému vedoucímu, Brunovi Jungwiertovi, za nápad na tuto diplomovou práci, jeho neocenitelné rady a připomínky k ní a za to, že mi věnoval svůj drahocenný čas. Taky bych chtěl poděkovat své rodině a kamarádům za jejich podporu.

Prohlášení

Prohlašuji, že jsem svoji diplomovou práci vypracoval samostatně s využitím informačních zdrojů, které jsou v práci citovány.

Brno 6. ledna 2016

....
Jakub Vulgan

Contents

Preface

Galaxies are considered cornerstones of the universe. The nature of these giant formations of stars, gas, dust and exotic dark matter and dark energy is known to us since the early 20th century. In 1960s, the first structural peculiarities have been observed and some of those have been faint arclike structures that came to be known as shells or ripples. These are not only interesting from the astronomer's point of view, but also beautiful to observe (see NGC 7600 in Fig. 1).

The boom in study of these shell galaxies came in 1980s with the development of better observational and image reducing techniques as well as computation capacity. First theories concerning their origin rose and one of them was merger model, which predicts collisions of galaxies. It was also proposed that from the look of the shell system, one can determine it's host galaxy's potential. This, however, proved to be too big of a task, so intense study of these galaxies was abandoned until recently, when the discovery of shells in exotic types of galaxies renewed the interest in them.

Our goal is to simulate the birth of a shell galaxy using radial encounter of high mass ratio galaxies (*minor merger*), determine the effect of different gravitational potentials on the results and try to incorporate gas into these simulations using sticky-particles method.

This thesis is divided into several parts, in the first one, we summarize known properties of shell galaxies and describe some theories of their origin. In the second part, we describe our model, potentials used and methods to simulate gas. And lastly in the third and fourth part, we describe the results of our simulations and try to draw some conclusions from them.

Figure 1: *R*-band galaxy-subtracted image of NGC 7600 from Turnbull et al. (1999).

Chapter 1

Shell Galaxies

For several decades after Hubble's *tuning-fork* classification (Fig. 1.1), it has been thought that the shape of a galaxy is determined only by its type. Only after the advancement of observational techniques did astronomers notice structural peculiarities. The first attempt to catalog galaxies with these peculiar features was made by Arp (1966). The catalog contains 338 galaxies with shell galaxies numbered Arp 227 - 231 (Fig. 1.2) and labeled "concentric rings". The term shells is for the first time used in description of Arp 330.

The first catalog consisting of only shell galaxies was created by Malin and Carter (1983). Authors present 137 galaxies with declination ranging from $-90°$ to $-17°$ that show shell-like or ripple-like structures. They distinguish these as new type of galaxies - shell galaxies. Authors describe them as such: "These galaxies appear at first sight to be normal ellipticals, but closer inspection reveals one or more edge-brightened structures either in the optical envelope or (more often) beyond the discernible limits of the elliptical galaxy. The shells may be somewhat diffuse; generally however, they are sharp-edged and may be associated with other disturbances within the envelope" (Malin and Carter, 1983, p. 534).

Authors give us statistical information about their catalog: about 10% of the analyzed early-type galaxies (Hubble types E, E/S0, S0) contain shells. Out of 137
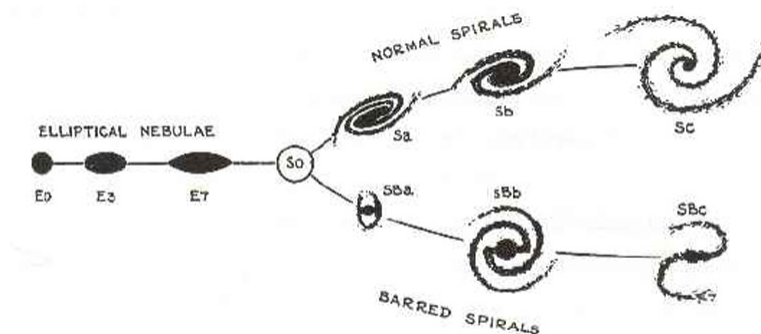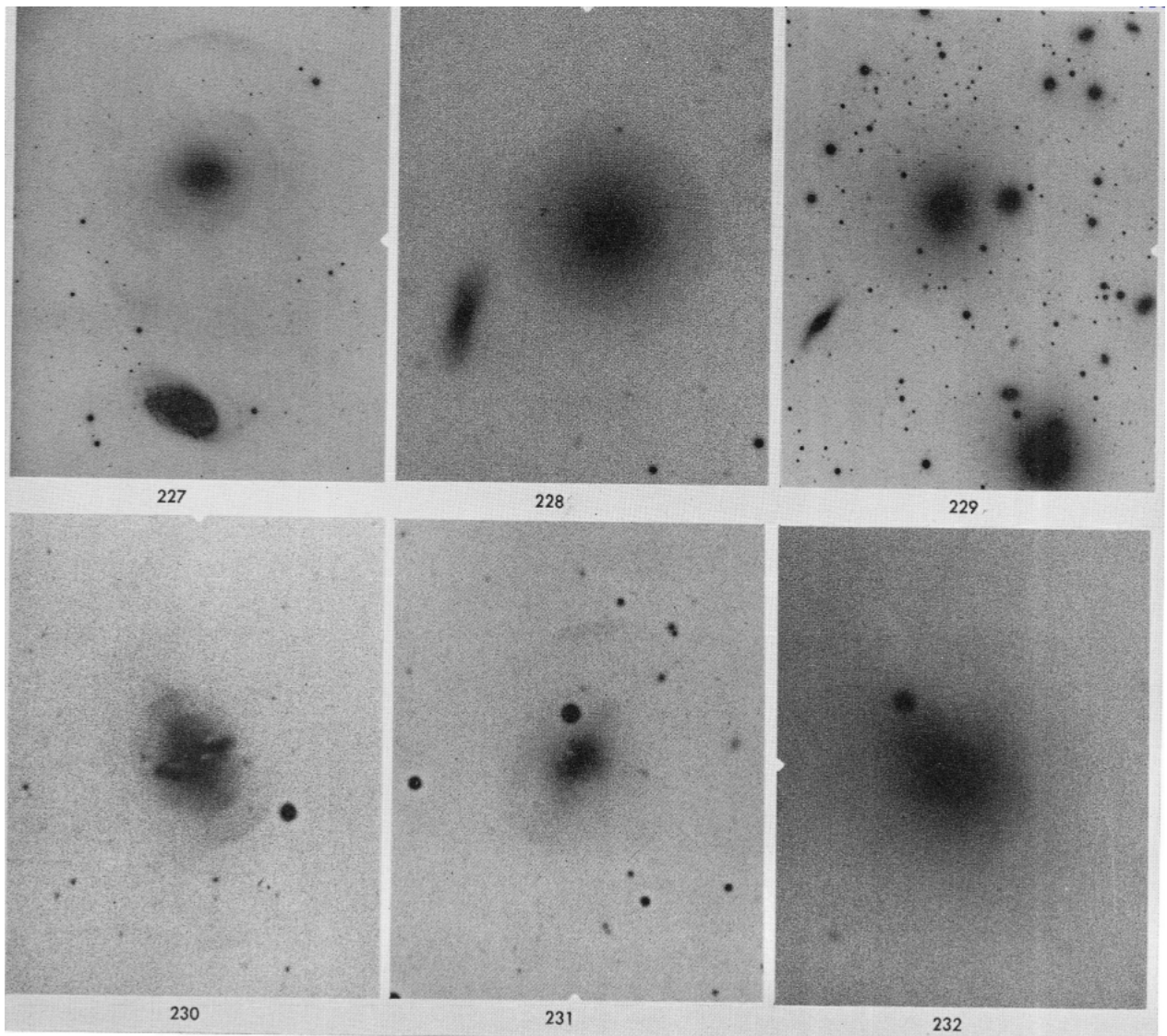

Figure 1.1: The Hubble sequence. From Hubble (1936)

Figure 1.2: Shell galaxies Arp 227 - 231. From Arp (1966)

identified shell galaxies, 65 (47%) are isolated, 42 (31%) occur in loose groups, only 5 (4%) occur in clusters and the remaining 25 (18%) occur in groups of two to five galaxies. This would suggest that shells do not occur in high galaxy density regions. Authors explain this by the fact that the tidal effects of other galaxies rapidly disrupt the shell structures, or because the collisions between galaxies, which lead to shell formation are low velocity encounters, and high galaxy density regions are also regions of high relative velocity (Malin and Carter, 1983, p. 538).

Schweizer and Seitzer (1988) discovered that shells can occur not only in early type galaxies, as it was believed, but also in disc galaxies of types S0/Sa, Sa and even in Sbc galaxy. Authors also prefer using term ripples to shells because it's more descriptive and it does not force a particular geometric interpretation.

Quinn (1984) summarized multiple studies of shell galaxies into several points:

1. Shells have been detected both photographically and photoelectrically around normal ellipticals and abnormal ellipticals. The number of shells around each galaxy ranges from one to approximately 20.

2. The shells are sharply defined, arclike with similar curvature for all shells, hence the structures are presumably 3-D.

3. Shells occur over a large range of radii.

4. The shells form incomplete, nearly concentric, arcs and rarely completely encircle the central galaxy.

5. Shells in general appear to be interleaved in radius. That is, the next outermost shell is usually on the opposite side of the nucleus.

6. In the case where central galaxy has a pronounced eccentricity, the shells tend to be aligned with the optical major axis of the galaxy.

7. Shell galaxies occur most often in regions of low galactic density.

1.1   Appearance of shells

Shells are of *stellar nature* and as stated in Quinn (1984), they have sharply defined edges and form arclike structures encircling the host galaxy. Shell systems have been observed with various numbers of shells, appearances and distributions. A large fraction of the Catalog of elliptical galaxies (see Malin and Carter, 1983) consists of galaxies with less than 4 shells. Rich systems with approximately 30 shells (e.g. NGC 3923) are rather rare. Given the fact, that shells actually are faint and contain only a fraction of the host galaxy's total luminosity (3-6%, surface brightness contrast of 0.1-0.2 mag) it's sometimes difficult to even detect them.

Prieur (1990) and Wilkinson et al. (1987) recognized three different morphological types of shell galaxies.
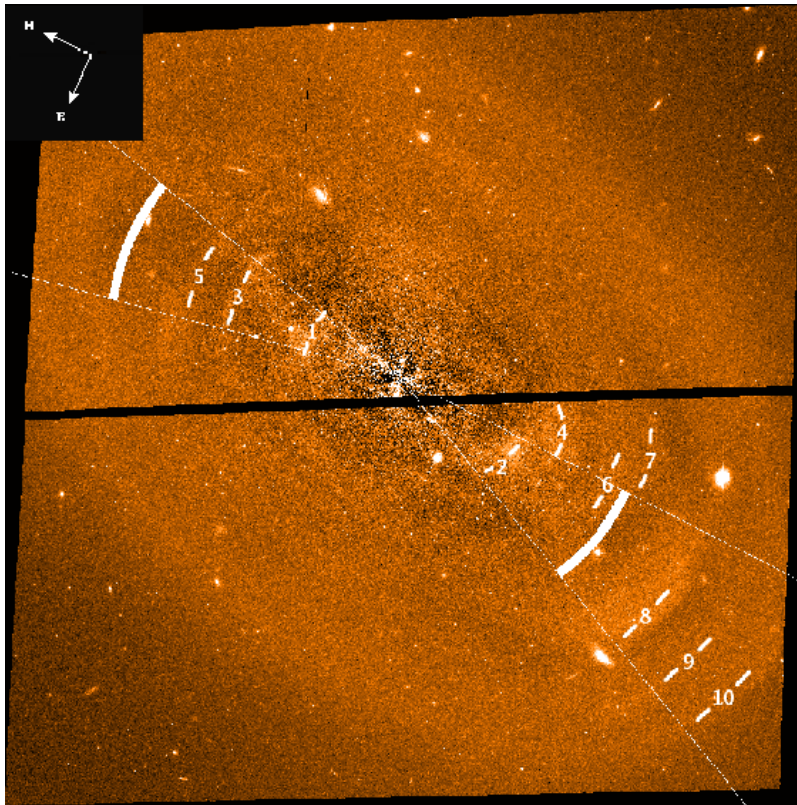
Figure 1.3: Type I shell galaxy NGC 1344 from Sikkema et al. (2007)

- **Type I (Cone)** - Shells aligned with galaxy major axis and interleaved in radius on alternate sides of galaxy. Examples are NGC 3923, NGC 1344 (Fig. 1.3).

- **Type II (Randomly distributed arcs)** - Shell are randomly distributed around rather circular galaxy. Example is NGC 474 (Fig. 1.4).

- **Type III (Irregular)** - Shell structure is more complex or there are too few shells to be classified.

Observations suggest that all three types occur evenly.

The ratio between the distance from the galactic center to the outermost shell and the innermost shell is defined as *radial range* of the shell system. It is number often used to describe the shell galaxy. However it's values range from rather high for the type I shell galaxies (60 for NGC 3923) to more typically 10 or less. For galaxies with very few detected shells, the value is even less than 5.

As for the angular distribution of the shells Dupraz and Combes (1986) state that it is strongly related to the eccentricity of the host galaxy. When the elliptical is nearly E0, the structures are randomly distributed around the galactic center. On the contrary, when the galaxy appears clearly flattened (>E3), the shell system tend to be aligned with its major axis and interleaved in radius on both sides of the center.
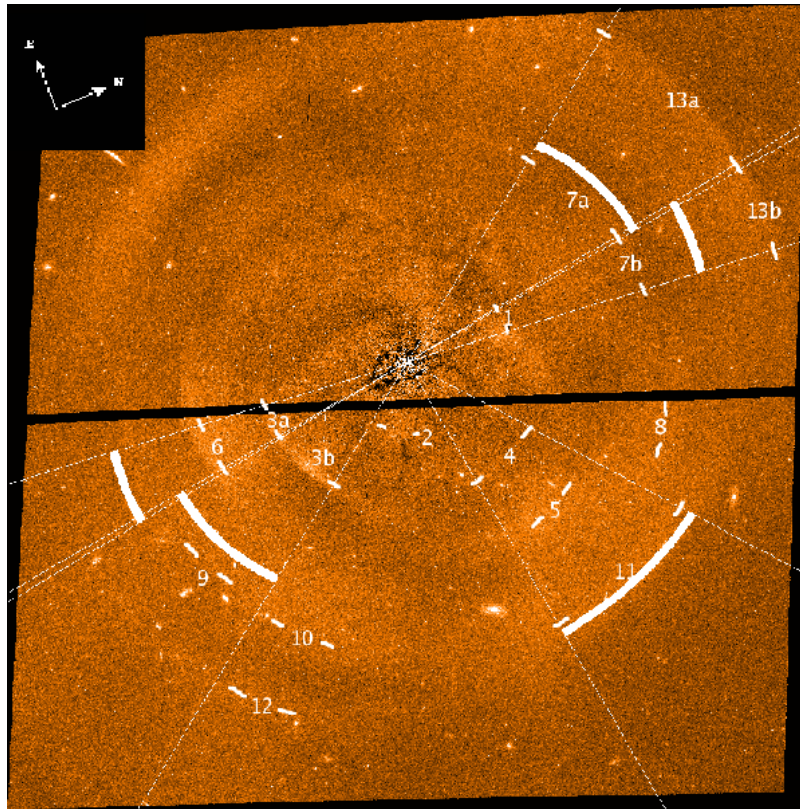
Figure 1.4: Type II shell galaxy NGC 474 from Sikkema et al. (2007)

Fort et al. (1986) state that the characteristic thickness of the shells are of order 10% or less of their distance from the center of the galaxy.

In the late 80's, the interest in shell galaxies slowly faded, however in recent decade, multiple new researches have been conducted. This was caused by discovering shell structures in a galaxy hosting quasar (Canalizo et al., 2007), in M31 (Fardal et al., 2007, 2008) and in dwarf galaxy in the Fornax constellation (Coleman et al., 2004). Helmi et al. (2003) state that ringlike structures observed in many galaxies, including our own, are also thought to be of analogical origin, as shells.

As for the color of the shells, it has been discovered that there are differences in the color of the shells and of the host galaxy. From the beginning of the research on shell galaxies, it was believed that they are rather bluer than the host galaxy. However, given their low surface brightness contrast, it has been rather difficult to obtain data.

Carter et al. (1982) present us with optical and near-IR photometry of NGC 1344. Derived color indices are $B - R = 1.2 \pm 0.3$, $B - H = 3.07 \pm 0.27$ for shells and $B - R = 1.60 \pm 0.15$ and $B - H = 3.84$ for the center of the galaxy. Multiple authors found the same tendency for the shells to be bluer than the center.

Pence (1986) focused on NGC 3051 and NGC 3923 and found out that color indices for the shells and the center of the galaxy differ only marginally and, therefore, confirmed earlier work of Fort et al. (1986). However, reddening of shells towards

the center of the galaxy was discovered.

Recent works show that the assumption of blue shells might be wrong, and that in fact, it's quite the opposite. Sikkema et al. (2007) discovered the shells to be slightly more red than the center of the galaxy in five out of six studied galaxies (red: NGC 1344, NGC 3923, NGC 5982, NGC 2865, NGC 7626; blue: NGC 474). Authors attribute the red color to dust physically connected to stellar shells.

1.2 Gas and dust

Schiminovich et al. (1994) presented discovery of arcs of atomic gas HI parallel to stellar shells, but shifted 1 arcmin to the outside of them in Cen A. Later, similar shift of HI arcs was also discovered in NGC 2865 (Schiminovich et al., 1995). Schiminovich et al. (1997) presents us with a study of HI gas in 8 shell galaxies (NGC 474, 5018, 7135, 1210, 2865, Arp 230, MCG -5-7-1, NGC5128). The latest study of Arp 230 and MCG -5-7-1 in Schiminovich et al. (2013) suggests, that these galaxies provide evidence of recent accretion, with gas and collisionless stars showing clear associations, though the displacement suggests the presence of significant gas-dynamical interaction.

Charmandaris et al. (2000) presents us with a study of molecular gas in the shells of Cen A. Authors detect CO emission from two of the fully mapped optical shells with associated HI emission, indicating the presence of H_2, assuming the standard CO to H_2 conversion ratio. All structures can be seen in Fig. 1.5

1.3 Simulations of gas

The first simulations of galactic mergers with gas were carried out by Weil and Hernquist (1993). These simulations use Smoothed Particle Hydrodynamics method in rigid potentials with secondary potential being shut down at the time of disruption. Results suggest, that stellar and gaseous component are segregated and form different structures - stars form shells whereas gas forms dense rings around nucleus of the primary galaxy where massive star formation may occur. That is in line with observations, where about 20% of shell galaxies exhibit nuclear post-starburst spectra.

Contrary to previous work, Kojima and Noguchi (1997) used self-graviting systems for both galaxies with gas being simulated by sticky-particles method. No segregation of stellar and gaseous components is shown in this work. Star formation is mainly reduced because of scattering on deep potential well of primary in case of radial and retrograde encounter. In case of prograde encounter, inner parts of secondary survive the merger and a small bar is created, that causes bar-driven gas inflow and strong starburst.

Combes and Charmandaris (2000) distinguish diffuse HI gas and small and dense gas that has intermediate behavior between stars and HI. In their simulation, dynamical friction is taken into account and the outcome is, that gaseous component is liberated first since it is less bound than stars and then, stars lose energy due to
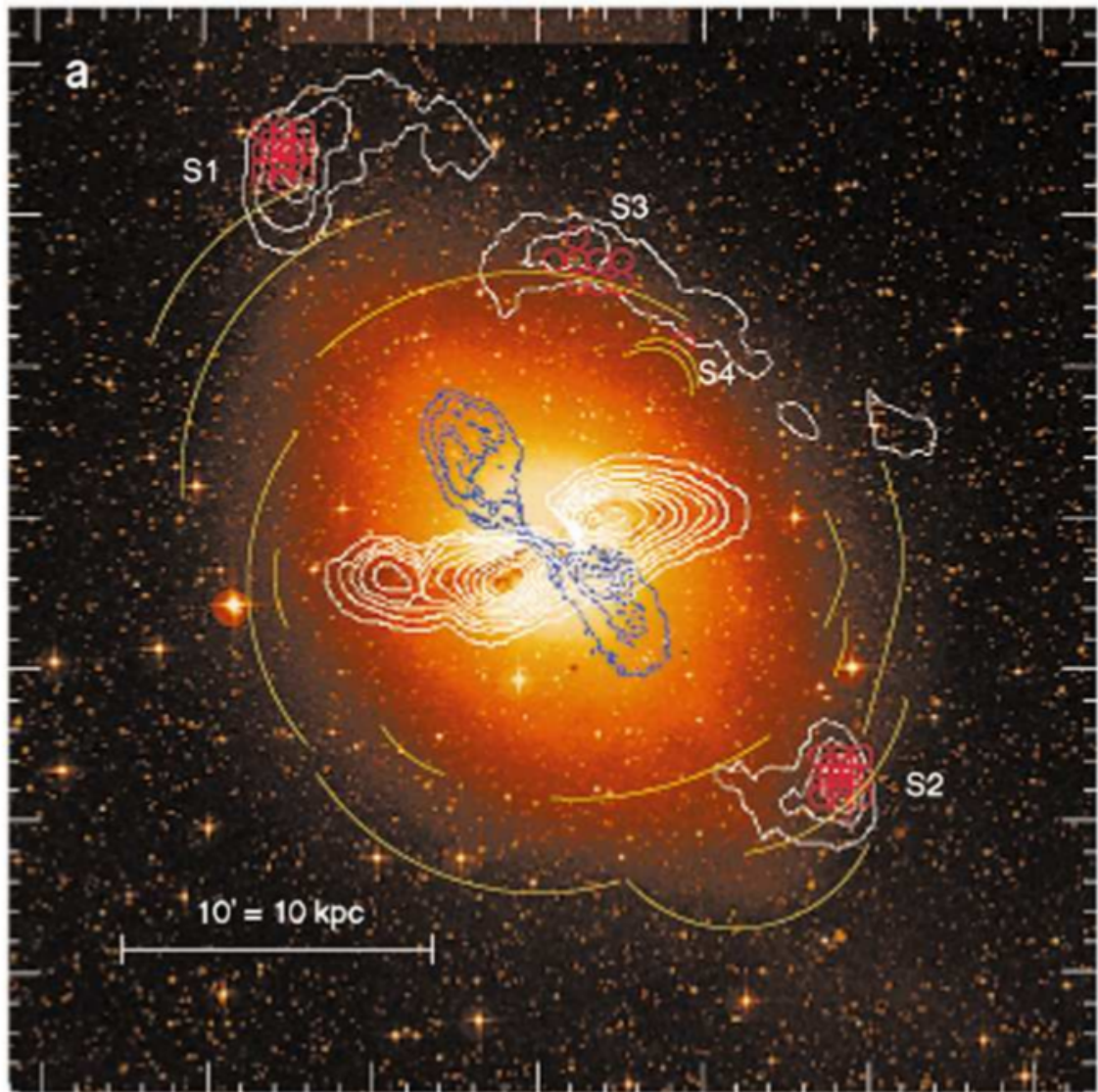
Figure 1.5: A Digitized Sky Survey optical image of Cen A with the contours of HI gas superimposed in white. North is up and east is to the left. The positions observed in CO are marked with the red circles. The locations of the outer stellar shells are underlined by the yellow solid lines. The inner 6cm radio lobes are depicted by the blue contours. Note the jet alignment with the location of the CO detections. The outer radio lobes are far more extended. From Charmandaris et al. (2000)

dynamical friction. This explains the displacement of the gaseous and stellar shells observed in some shell galaxies discussed in Part 1.2.

1.4 Origin of shell galaxies

Since the discovery of shell galaxies, astronomers and physicists have been perplexed by their potential origin and many theories rose over the years. In next part, we will present some of them.

1.4.1 Internal origin

The first attempt to explain the origin of shell galaxies comes from Fabian et al. (1980). Authors suggest that shells are regions of recent star formation in a shocked galactic wind. This theory was later expanded by Williams and Christiansen (1985). In their model, the galactic interstellar medium is blasted out by explosions in an active nucleus phase early in the history of the galaxy. This gas later creates shell, that expands, cools down by radiation and thins down until fragmentation occurs and star formation begins. After some time, stars with big enough mass explode as supernovae and restart the whole process again. This way, several generations of shells can be created.

Another theory was suggested by Kundt and Krause (1985). This theory also assumes the existence of an active nucleus, which ejects several gaseous shells. These create filamentary structures that form the shells.

Many more theories were suggested but most of them were not proven by observations. Even nowadays, we're not certain about the origin of shells. However two major theories remain plausible - weak interaction model and merger model.

1.4.2 Weak Interaction Model

The WIM theory was suggested by Thomson and Wright (1990), when they rejected the merger model 1.4.3. Authors present shells as density waves induced in a thick disc population of dynamically cold stars by a close encounter of two galaxies on a parabolic trajectory. Numerical simulations show, that model creates 3-D structures, that after projection exhibit sharp outer edges. Final shape of shells is determined by distance of the galaxies and their masses.

Big advantage of this model is, that shell galaxies of type I and II are created by the same process, the only difference is projection. Shells are visible from every angle, when viewed at inclination less than $60°$ the system seems as type II, when viewed at inclination larger than $60°$ it looks like type I. The theory also gives correct relative frequency of these two types. The observed correlation between eccentricity of galaxy and angular distribution of shells can also by explained by projection effects and the theory suggests, that shells galaxies must be oblate spheroids. Finally, the model is in agreement with observed shells interleaved in radius.

The consequence of WIM is the fact, that stars must have almost circular trajectories and, thus, authors expect radial velocities consistent with radial velocities

measured in thick disk observed edge-on. On the other hand, the merger model 1.4.3 predicts radial trajectories for stars creating shells. Thus the presence of rotational movement could theoretically show, which model is the right one. The necessity of thick disc is one of major disadvantages of this model, because ellipticals are known for being dynamically hot systems.

1.4.3 Merger Model

The idea of shells being connected to mergers was suggested for the first time in Schweizer (1980). A few years later, mathematical model for this theory was described in Quinn (1984).

Author describes merger of a massive elliptical primary and a disc secondary galaxy. From the low relative surface brightness of shells compared to the center of galaxy, low relative mass of the secondary can be derived. One can therefore use model of a static potential well and use the N-body simulation. Mechanism of the merger depends heavily on an orbital angular momentum of the merger.

In case of low orbital angular momentum of the merger, process called phase-wrapping ensues. One dimensional case can be seen in Fig. 1.6. Particles creating small secondary galaxy begin to oscillate in the potential of a primary galaxy. In their turning points, the particles have slowest speed and therefore spend most of their time there, creating density maxima. The most tightly bound particles reach these maximal radial positions first, but as more distant particles reach their turning points, the density wave propagates slowly in radius. The wrapping proceeds at a rate determined by the range in periods present, and the number of wraps at time t after the initial infall is

$$N = \frac{t}{2\pi}(\Omega_{\max} - \Omega_{\min}), \tag{1.1}$$

where Ω is the radial frequency and $\Omega_{\max}$ and $\Omega_{\min}$ are the maximum and minimum frequency present, respectively. Phase-wrapping explains shells interleaved in radius as well as their number, which is simply proportional to the time passed from the merger (see eq. (1.1)).

In case of high orbital angular momentum the merger is predominantly nonradial. For the general case of an inclined disc, the difference between periods across the disc causes it to shear. Process similar to phase-wrapping called spatial wrapping ensues. Structures created by this process however exhibit characteristic not in accordance with the observed shells: (1) When viewed from a point in the orbit plane of the disc, the structures are not shell-like but tend to be pointed and confused. (2) The structures quite often overlap and have appreciably different curvatures. (3) Since the density enhancements of spatially wrapped disks are due to projection effects, the enhancement is predominantly uniform in azimuth and the shells appear enclosing. For the reasons above, author suggests that shell galaxies are created only in radial encounters (Quinn, 1984, p. 603).

Another work on the topic is presented by Dupraz and Combes (1986). Authors study mergers between a massive elliptical and both spiral and elliptical secondary of mass approximately 1% of the primary. They conclude that the simulations can fit the radial distribution only with the additon of an extended component of dark
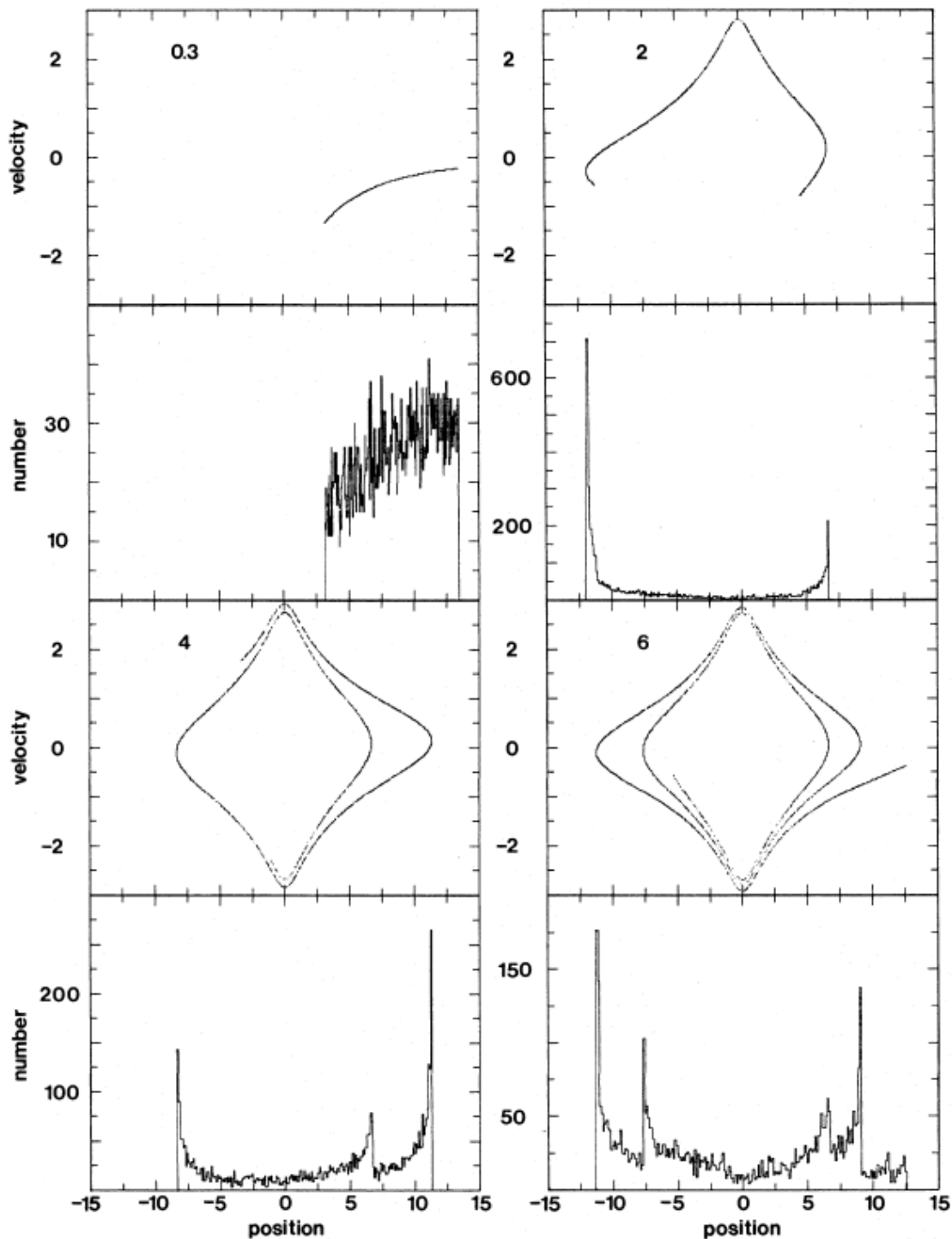
Figure 1.6: The phase space and configuration space time evolution of 5000 test particles falling from rest into an isochrone potential. The numbers in the top left of each phase plot are the time passed in units of the radial period of the most tightly bound particle. The configuration space distribution of the particles at each time is shown directly below the corresponding phase plot. Positions are in units of the isochrone scale length, and velocities are in units of $(\mathrm{G}M/10a)^{1/2}$, where M is the total mass and a the scale length. From Quinn (1984).

matter or halo in the potential (for the well studied NGC 3923, the minimum mass ratio between the dark and visible matter equals 20 inside 100 kpc). Shell geometry is heavily dependant on the 3-D shape of the primary. For a prolate galaxy, shells are aligned with the major axis and interleaved in radius, for an oblate one, two different shell-system geometries can occur, depending on the impact parameter of the companion: either the shell system forms a small angle about the symmetry plane, and shells are arcs of large angular extent, randomly spread around the galaxy; or, though with a lower probability, the shells are aligned with the minor axis. When avereging over all impact parameters and projection angles, the probability to see shell is approximately 60% around prolate and approximately 20% around oblate galaxy. When comparing companions, for the elliptical secondary, shells have lower contrast, are more regular than for the spiral secondary. Furthermore, there are no other features such as filaments and spokes present. Radial distribution and geometry of the shells are independent of the companion type. Thus they conclude, that it could be possible to determine the potential of the primary from the its shell system. Authors, however, do admit, that their simulations yield much lower range of radii for the shells than observed and suggest introducing dynamical friction to the simulations to solve the problem.

Hernquist and Quinn (1988, 1989) simulate different types of mergers and discuss their findings. In their first work, they concentrate on massive low-mass systems encountering massive spherical galaxies. Mergers could be radial or nonradial and the secondary could be spherical or disc galaxy. General conclusions are (1) Nonradial encounters can result in creation of shells as well and (2) Spherical secondary results in sharper and more symmetrical shell system than that of disc secondary. In the second work, they again simulate radial and nonradial encounters but in this case, the primary potential is nonspherical. They conclude that it is possible to create shells even in spiral galaxies, however their morphology is sensitive to the shape of the primary at large and small radii as well as the detailed structure of the companion. Thus it is difficult, if not impossible, to infer the form of the primary potential from the shell geometry alone and in this conclusion, authors disagree with Dupraz and Combes (1986). After this work, the interest in shell galaxies started to fade.

Recently, however, new papers on shell galaxies started to emerge. Canalizo et al. (2007) studied galaxy containg quasar MC2 1635+119 with N-body simulation and from the location of the furthest shell, they determined time of the merger to be 100 million to 2 billion years ago, which suggests causal connection between the merger and the start of the quasar activity.

Ebrová et al. (2010) showed that time derived from the position of shells can be severely underestimated when not taking dynamical friction and gradual disruption of the secondary into account. The position of the outermost shells remained the same, its luminosity however lowered rapidly, which leads to detection difficulties and possibility of missing it in observations. The time derived from the position of the second outermost shell was in this particular case two times lower than the time derived from the outermost shell.

Chapter 2

Our model

In all the simulations we assume the merger origin of the shells, in this case *minor merger*. Given the high mass ratio of the galaxies, secondary's distortion of primary's gravitational field is negligible. Therefore we can approximate combined field with appropriate analytical potentials. Star component is simulated by non-interacting *test particles* and the gas component can dissipate energy through encounters based on *sticky-particles* scheme (see 2.4).

In the beginning we started from the source code MERGE 09 provided by Bruno Jungwiert (2006, unpublished). The program is written in FORTRAN and uses graphical library PGPLOT written by Tim Pearson.

2.1 Integration of the equations of motion

The interaction between test particle of mass m and location $\boldsymbol{r}$ and potential ϕ is described by Newton's equation of motion

$$m\boldsymbol{r} = -\nabla\phi. \tag{2.1}$$

This equation cannot be generally solved analytically and numerical integration is needed. One of the most used methods is *Leapfrog* algorithm. This method works with velocities derived for a half time step earlier or later than current positions. By doing so, the accuracy of the computation is increased by an order compared to the case if positions and velocities are taken simultaneously. It's also *symplectic integrator* which means it conserves mean values of some integrals of motion e.g. total energy of the system.

The Leapfrog integrator works like this: from the initial positions $\boldsymbol{r_0}$ we compute acceleration $\boldsymbol{a_0}$ and use it to compute velocity half step backward

$$\boldsymbol{v_{-1/2}} = \boldsymbol{v_0} - \boldsymbol{a_0}\frac{\Delta t}{2}, \tag{2.2}$$

where Δt is the time step. After that the algorithm for updating velocity and position

is

$$\boldsymbol{r_i} = \boldsymbol{r_{i-1}} + \boldsymbol{v_{i-1/2}}\Delta t$$
$$\boldsymbol{a_i} = f(\boldsymbol{r_i})$$
$$\boldsymbol{v_{i+1/2}} = \boldsymbol{r_{i-1/2}} + \boldsymbol{a_i}\Delta t. \tag{2.3}$$

2.2 Plummer potential

All the simulations were carried out for spherically symmetrical potentials. First of those was *Plummer potential* which was first used by Plummer (1911) to fit observations of globular clusters but for its simple expressions of dynamical quantities it's been widely used in galactic astronomy as well. Radial dependency of density is

$$\rho(r) = \left(\frac{3M}{4\pi b^3}\right)\left(1 + \frac{r^2}{b^2}\right)^{-\frac{5}{2}}, \tag{2.4}$$

where M is mass of the object and b is Plummer radius, a scale parameter that determines compactness of the galaxy.

Poisson's equation ties together potential and density

$$\nabla^2\Phi = 4\pi G\rho \tag{2.5}$$

and we get expression for gravitational potential

$$\Phi(r) = -\frac{GM}{\sqrt{r^2 + b^2}} \tag{2.6}$$

where G is gravitational constant. Note that potential for $b = 0$ is the same as potential of a point mass.

2.3 Hernquist potential

The second potential used in our simulations is called Hernquist potential and was first described by Hernquist (1990). It was derived to closely approximate empiric de Vacouleurs $R^{1/4}$ law for elliptical galaxies. Its advantages are the same as Plummer potential's - its dynamic quantities are expressible in terms of elementary functions. However there's a big difference between the two profiles: Plummer potential has constant core while Hernquist potential has cusp in core (meaning its density or potential nears infinity at center).

Radial dependency of density is

$$\rho(r) = \frac{M}{2\pi}\frac{b}{r}\frac{1}{(r + b)^3}, \tag{2.7}$$

where b is Hernquist radius analogically to Plummer profile. Combined with Poisson's equation (2.5) we get potential

$$\Phi(r) = -\frac{GM}{r + b}. \tag{2.8}$$

Similarly to Plummer potential, for $b = 0$ the potential is the same as potential of a point mass.

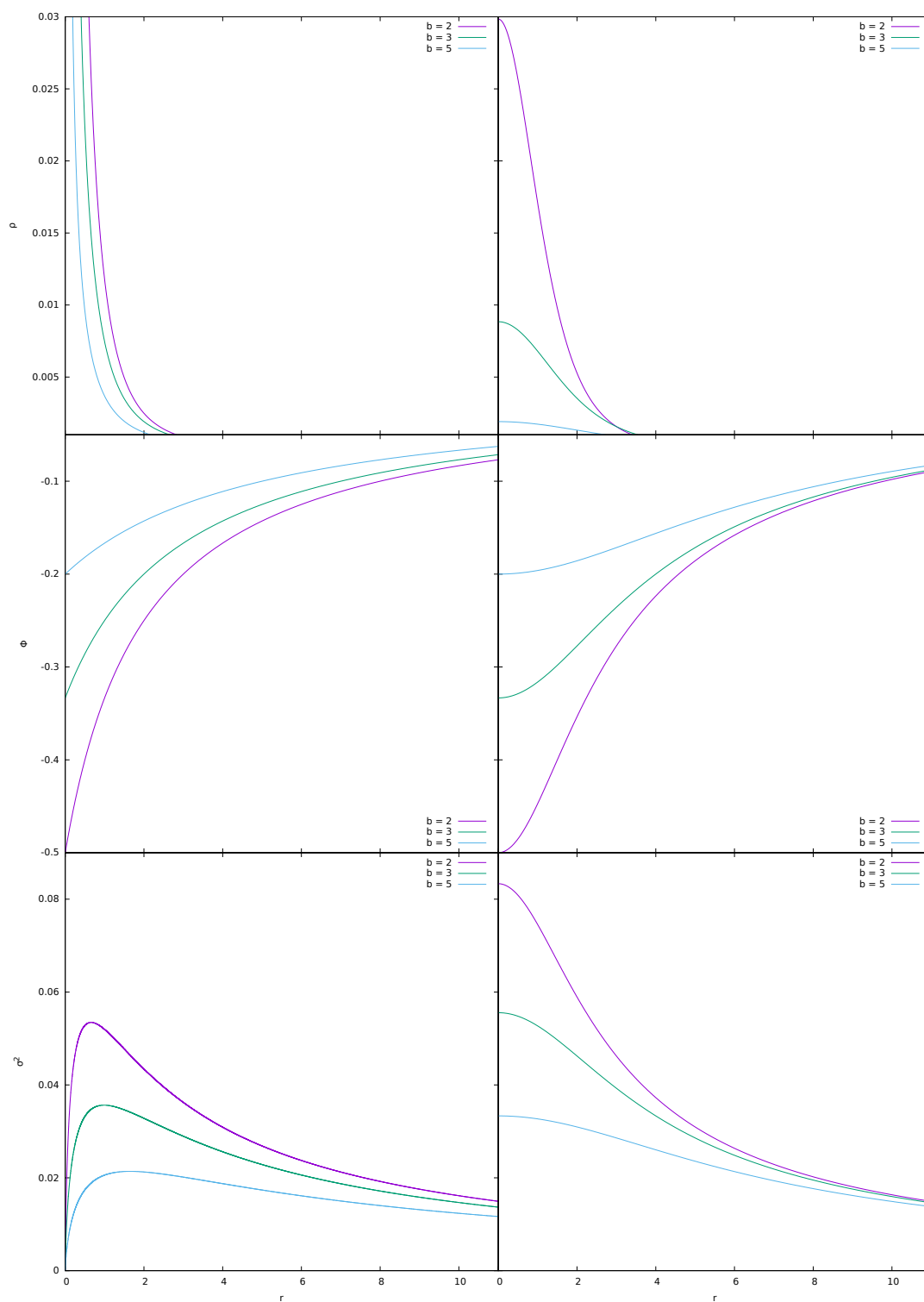Figure 2.1: Radial dependencies of density, potential and velocity dispersion for Hernquist (left) and Plummer (right) profile. Constants G and M are set to 1 and axes are in arbitrary units.

β_r	β_t	outcome
1	1	test particles, velocities don't change
0	0	inelastic collision, particles bond
-1	1	elastic collision, "billiard balls"

Table 2.1: Special cases of coefficients β_r and β_t.

2.4 Sticky-particles method

In our work hydrodynamics were simulated with sticky-particles method. This method works with discretely distributed gas particles that do not gravitationally interact with one another (so they are treated as test particles), however, they do interact during collisions when they can dissipate energy. Each particle has certain cloud radius R_{cl} (in our simulation, we chose for all particles to have the same cloud radius). After each integration cycle program searches for close enough particles and in case distance between two particles is less than $2R_{\text{cl}}$ and they move towards each other collision occurs. From center-of-mass frame, the relative velocities change according to these equations:

$$
\begin{aligned}
\boldsymbol{v_t^1} &= \beta_t \boldsymbol{v_t^0}, \\
\boldsymbol{v_r^1} &= \beta_r \boldsymbol{v_r^0}.
\end{aligned}
\tag{2.9}
$$

Velocities with upper index 1 are after collision, those with 0 are before. Indices r and t denote radial and tangential components of the velocity.

Coefficient β_r determines how much energy dissipates during collision. Dissipation occurs due to fact that the clouds collide at supersonic velocities and it gives birth to shock waves. Those can transform kinetic energy to internal energy of the clouds, which can be radiated out. In most simulations the β_r coefficient is chosen between 0.4 - 0.8. In our program we choose $\beta_r = 0.5$.

Coefficient β_t determines how much angular momentum is dissipated during collision. It happens mainly due to internal angular momentum of gas cloud. However in our simulations the clouds have zero angular momentum so there's no dissipation and we choose $\beta_t = 1$.

It's worth noting that there are special cases for some special choices of β_r, β_t. These are listed in table 2.1.

Equations (2.9) can be transformed from center-of-mass frame to more general inertial frame with the use of conservation of angular momentum and energy. The resulting equations are

$$
\begin{aligned}
\boldsymbol{v_1^1} &= \frac{1}{2}(\beta_t + 1)\boldsymbol{w} - \frac{\beta_t + \beta_r}{2}\frac{\boldsymbol{rw}}{r^2}\boldsymbol{r} + v_2^0, \\
\boldsymbol{v_2^1} &= \frac{1}{2}(\beta_t + 1)\boldsymbol{w} + \frac{\beta_t + \beta_r}{2}\frac{\boldsymbol{rw}}{r^2}\boldsymbol{r} + v_1^0, \\
\boldsymbol{w} &= \boldsymbol{v_1^0} - \boldsymbol{v_2^0}, \\
\boldsymbol{r} &= \boldsymbol{r_2^0} - \boldsymbol{r_1^0}.
\end{aligned}
\tag{2.10}
$$

Mass of the primary	$M_\mathrm{p} = 3.2$ x $10^{11}\mathrm{M}_\odot$
Plummer/Hernquist radius of the primary	$b_\mathrm{p} = 5$ kpc
Mass of the secondary	$M_\mathrm{s} = 3.2$ x $10^{9}\mathrm{M}_\odot$
Plummer/Hernquist radius of the primary	$b_\mathrm{s} = 0.5$ kpc
Initial radial distance of the galaxies	$D_\mathrm{ini} = 91.2$ kpc
Initial velocity of the secondary for Plummer potential	$V_\mathrm{ini,Pl} = 174$ km/s
Initial velocity of the secondary for Hernquist potential	$V_\mathrm{ini,Hq} = 169$ km/s

Table 2.2: Standard set of parameters for our simulations

Upper indices denote velocities before and after collision similarly to equations (2.9), lower indices denote number of particle.

2.5 Initial conditions

As stated before at the beginning of this chapter, we simulate minor merger i.e. merger of two galaxies with high mass ratio. We use spherically symmetric analytical potentials. In case of close encounter of the two galaxies, the secondary is tidally disrupted by primary's gravitational field. In our code, this is realized by setting the mass of the secondary to zero $M_\mathrm{s} = 0$.

In our work the mass ratio of the primary to the secondary is 100:1 and scale lengths of respective profiles are in primary-to-secondary ratio 10:1. Initial separation of galaxies of chosen high enough for the secondary not to be disrupted by primary's tidal forces and initial velocity is equal to escape velocity in that distance. Numerical values for the standard set of parameters used in all the simulations can be found in table 2.2.

Chapter 3

Simulations without hydrodynamics

In this chapter we attempt to simulate minor merger and subsequently manage to create shell galaxy. However, we are using just test particles that interact only gravitationally. These particles represent stars .

3.1 One particle

In the first simulation, we generated just one particle with only non-zero component of velocity being v_{x} and watched its trajectory when starting from different initial positions on y axis. As expected the particle started to move on non-closed trajectory called rosette. These are shown for Plummer profile (Fig. 3.1) and Hernquist profile (Fig. 3.2). It is clearly shown that the trajectories vary substantially for different y_0 and also between the two potentials.

When comparing Plummer and Hernquist potentials, the outcome is as expected. Particles on trajectories closer to the center of Hernquist potential are exposed to much stronger force pull due to the cuspy profile. That leads to their trajectories being more skewed and their apocenters laying at higher angles. This is shown on Fig. 3.3. Since according to merger model of origin, the shells are created by stars in their apocenters, difference shown between profiles should be seen in angular distribution of stars in their shells.

3.2 Stellar shells

After studying trajectories of one particle described in last section 3.1, we try to simulate the merger origin of shell galaxy. Both galaxies have their parameters listed in table 2.2. Secondary consists of 10^6 test particles and is truncated at 5 kpc. At time $T = 0$ the galaxies are separated only in x-axis and the secondary is moving towards the primary. The disruption of the secondary which is realized by setting mass of the secondary to zero occurs at about 300 Myr after the start of the simulation. The shells are created afterwards from stars of the secondary. This process in configura-
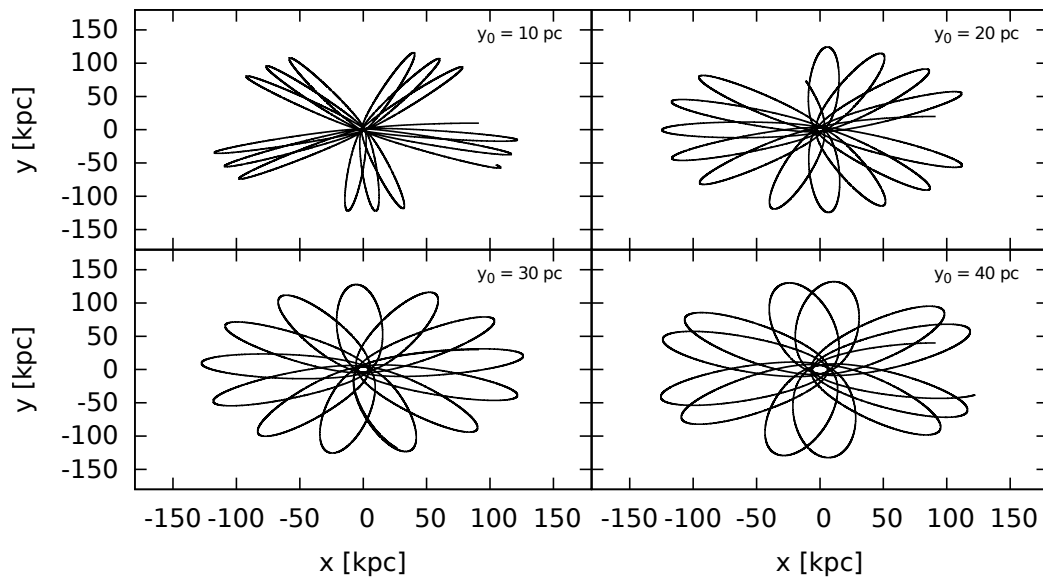
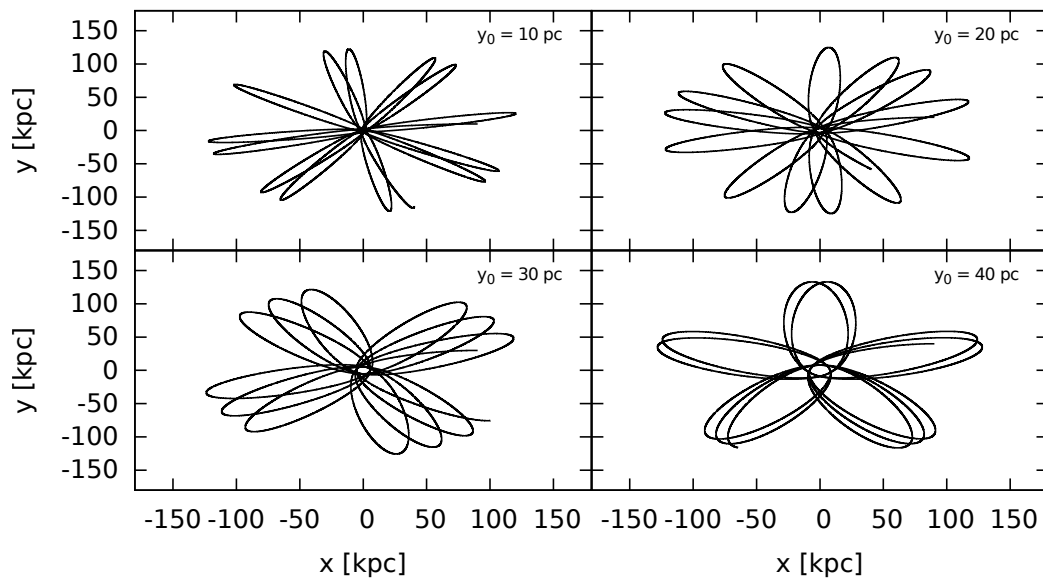Figure 3.1: Trajectories of a particle in Plummer potential for different y_0.

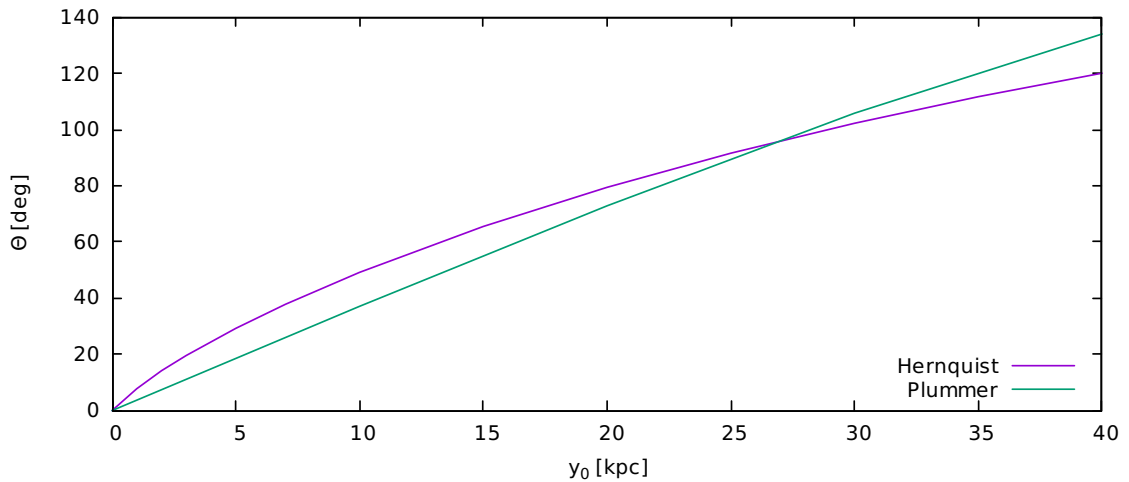Figure 3.2: Trajectories of a particle in Hernquist potential for different y_0.

Figure 3.3: Graph showing dependency of angular position (measured from $-x$ axis) of the first apocenter of trajectory θ on initial position y_0

tion space can be seen in Fig. 3.4 for the Plummer and in Fig. 3.5 for the Hernquist potential. In Fig. 3.6 and Fig. 3.7 the same process is seen in phase space.

The graphs in configuration space show that shells arise from the inner parts of the primary galaxy and then move outwards. Shells are interleaved in radius and aligned with major axis, therefore type I shell galaxy is created. The process of phase-wrapping is clearly demonstrated in graphs showing the phase space.

For easier identification of shells, histograms showing radial distribution of particles from the center of the primary are constructed. Such graphs are shown in Fig. 3.8. The radial distribution is different as expected. Shells in Hernquist potential are generally closer to the core of the primary and they tend to be brighter than the shells in Plummer potential. Furthermore, the distribution of test particles in distances $r > 100$ kpc si also significantly different. Test particles in Hernquist potential are more concentrated towards the center of the primary while particles in Plummer potential tend to reach greater distances. All of these properties should be observable in real galaxies.

To further quantify the difference in the radial distribution, graphs showing time dependency of the shell radii is created. From Fig. 3.9 we can see that there is no significant difference between Plummer and Hernquist potential other than shift in time. Given the fact that our simulation is considerably simplified, it is not possible to establish any observable conclusion.

One of our goals is to examine the angular distribution of particles creating the shells. This is accomplished by selecting particles which have distance from the center of the galaxy r in interval

$$(R_n - \Delta R_n) \leq r \leq R_n, \tag{3.1}$$

where R_n is the distance of the edge of the n-th shell determined from the radial distribution histogram and ΔR_n is the width of the n-th shell. In our work we choose
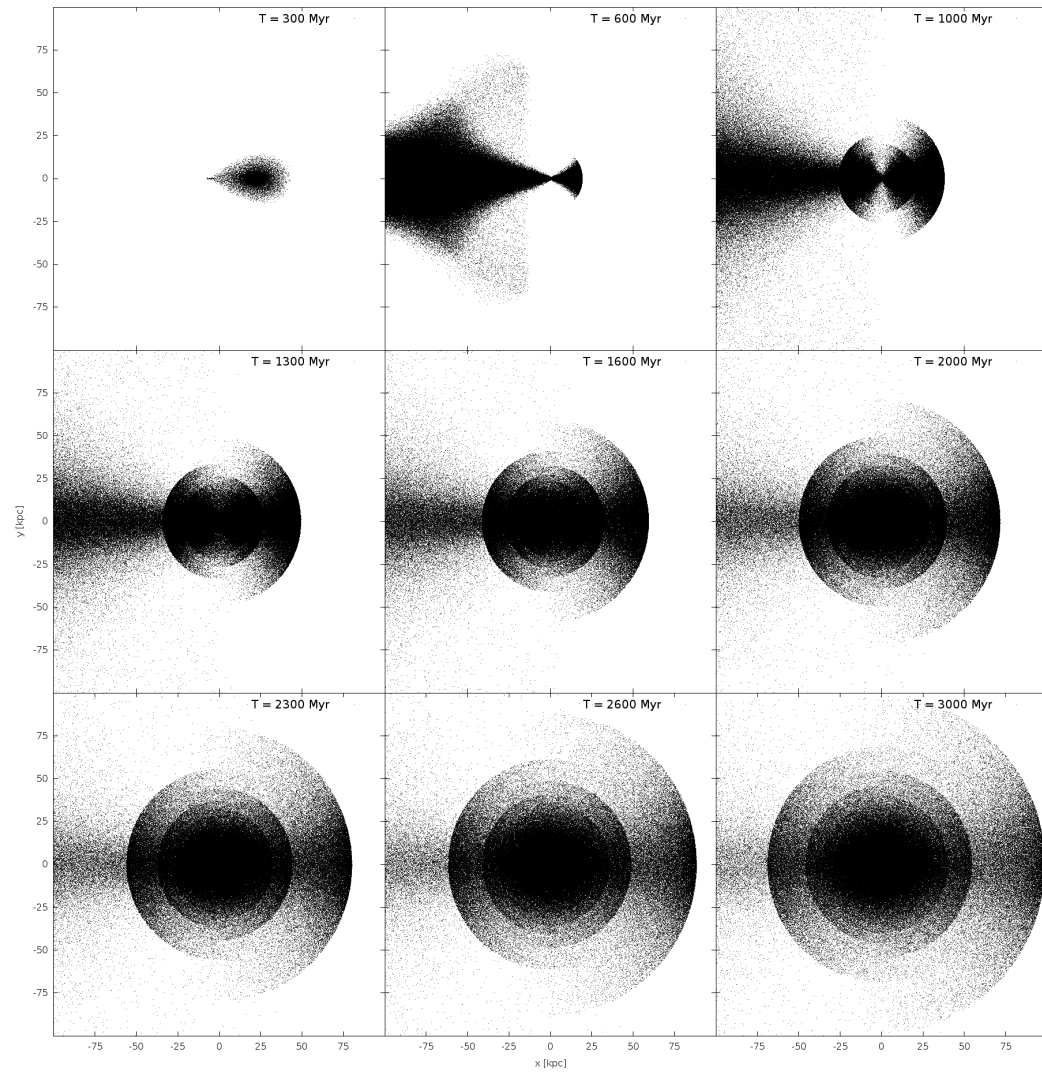
Figure 3.4: Simulation of the merger with Plummer potential shown in the configuration space x - y.
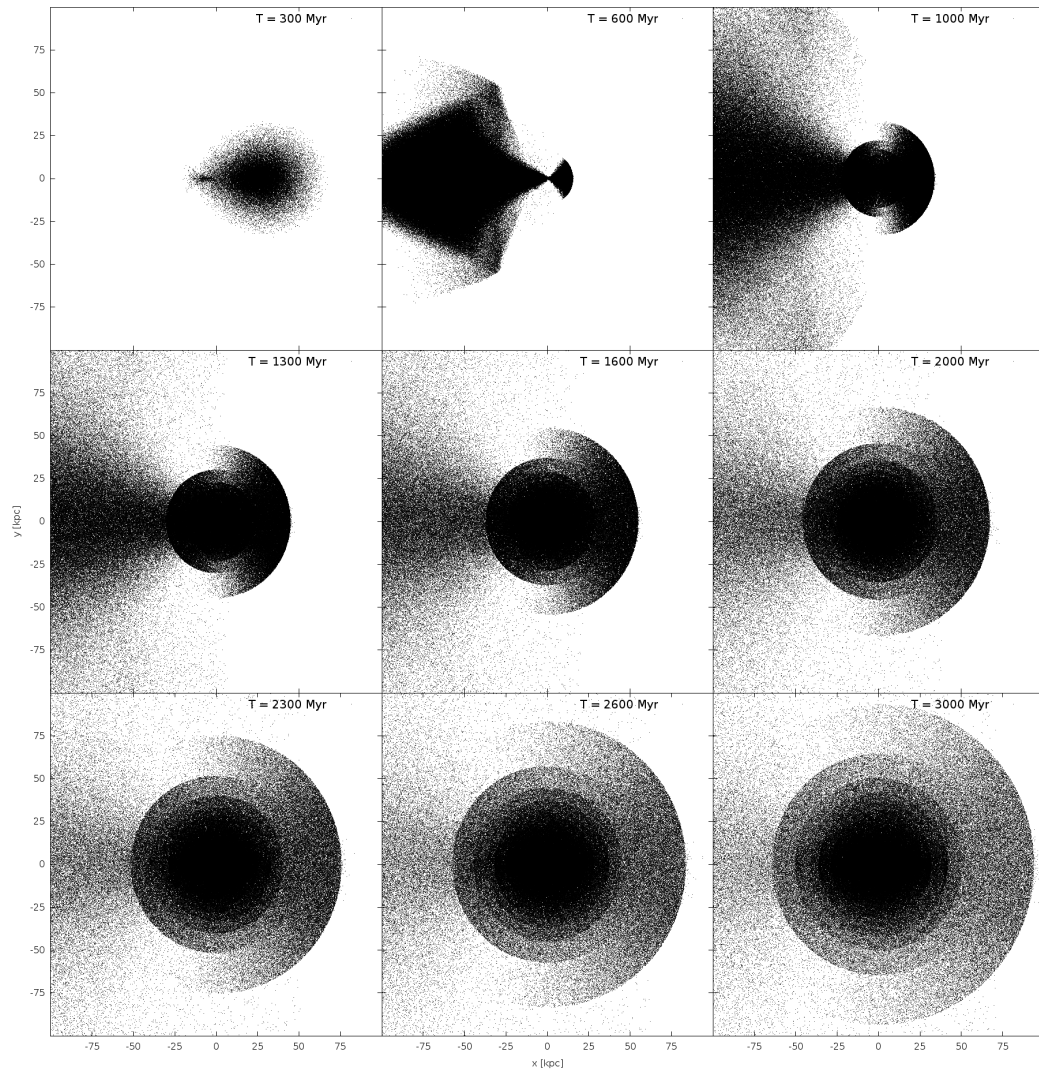
Figure 3.5: Simulation of the merger with Hernquist potential shown in the configuration space x - y.
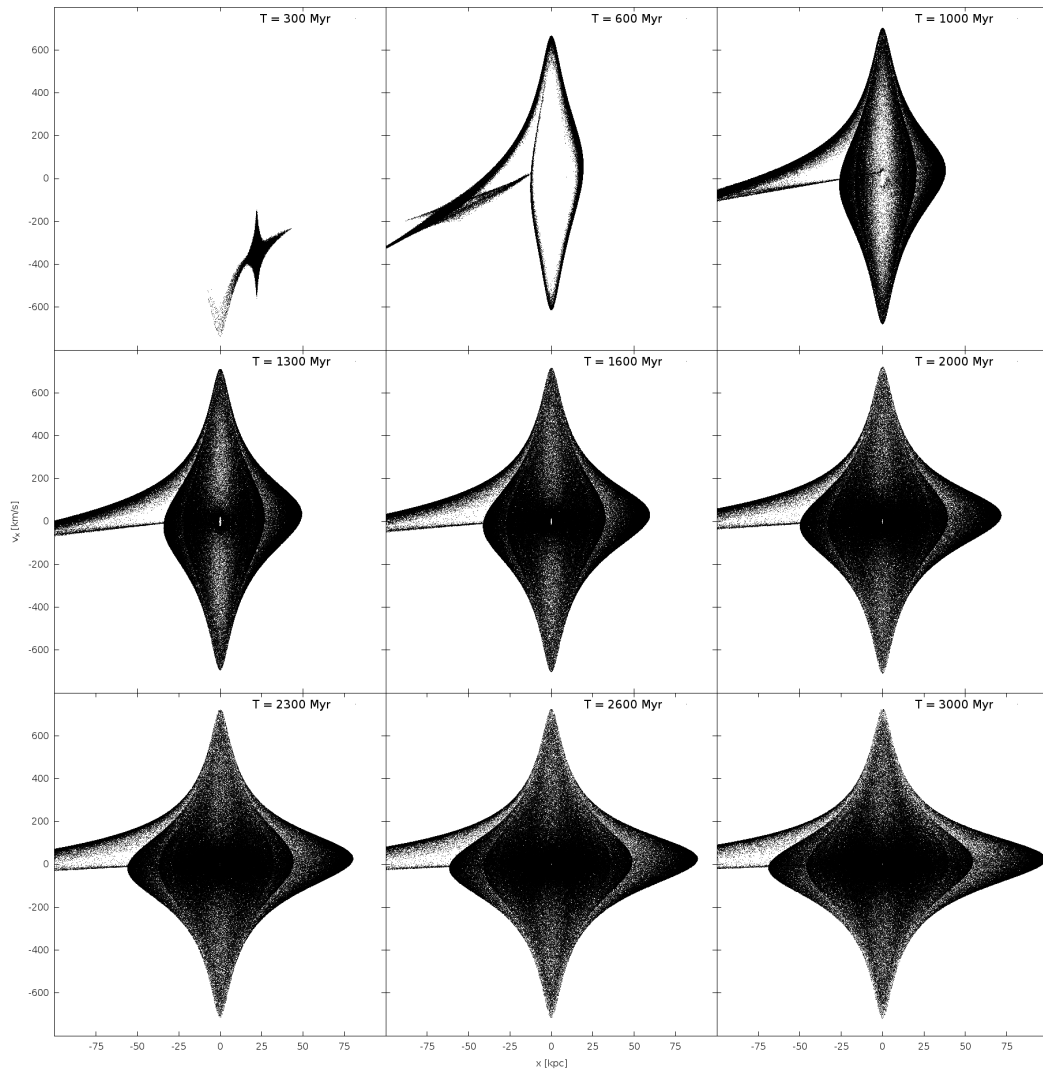
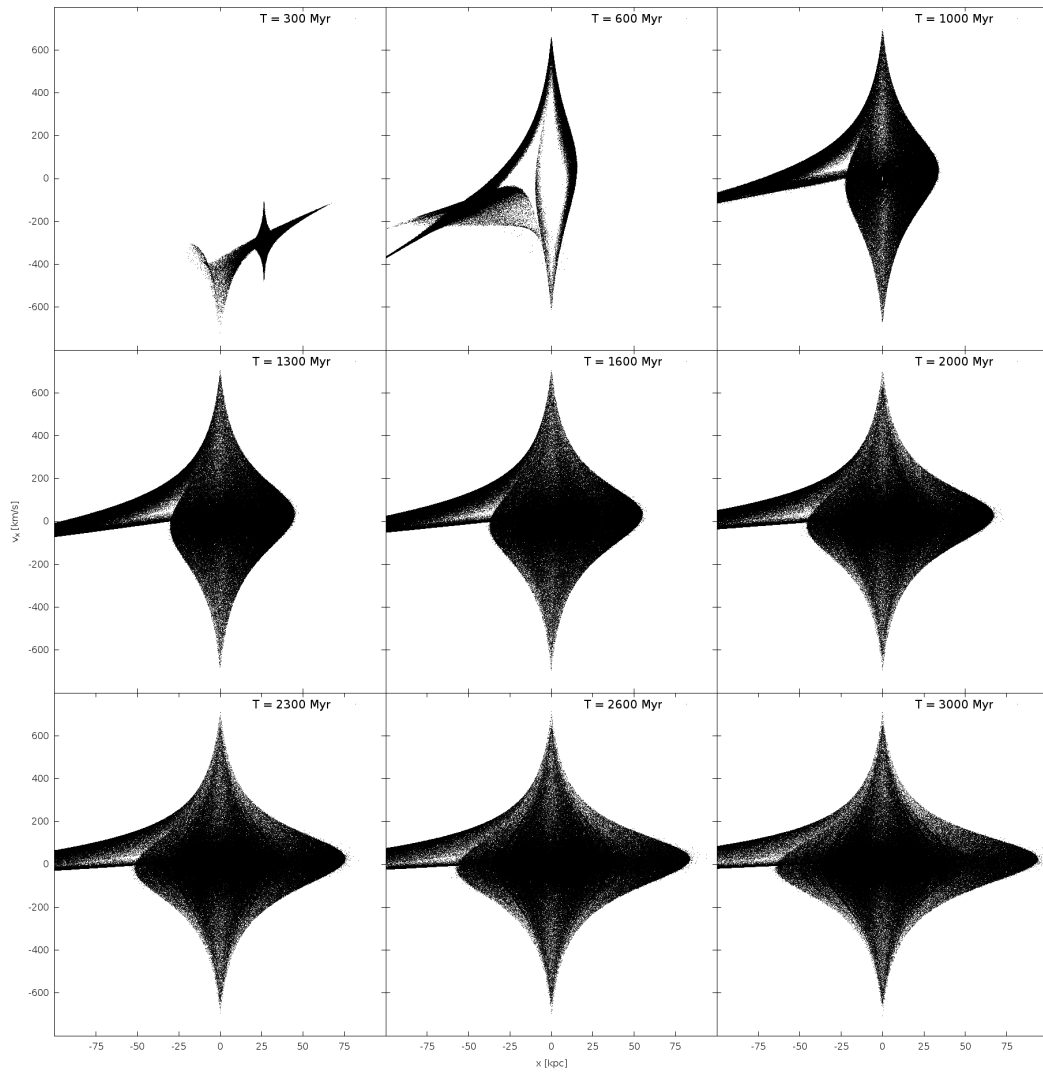Figure 3.6: Simulation of the merger with Plummer potential shown in the phase space x - v_x.

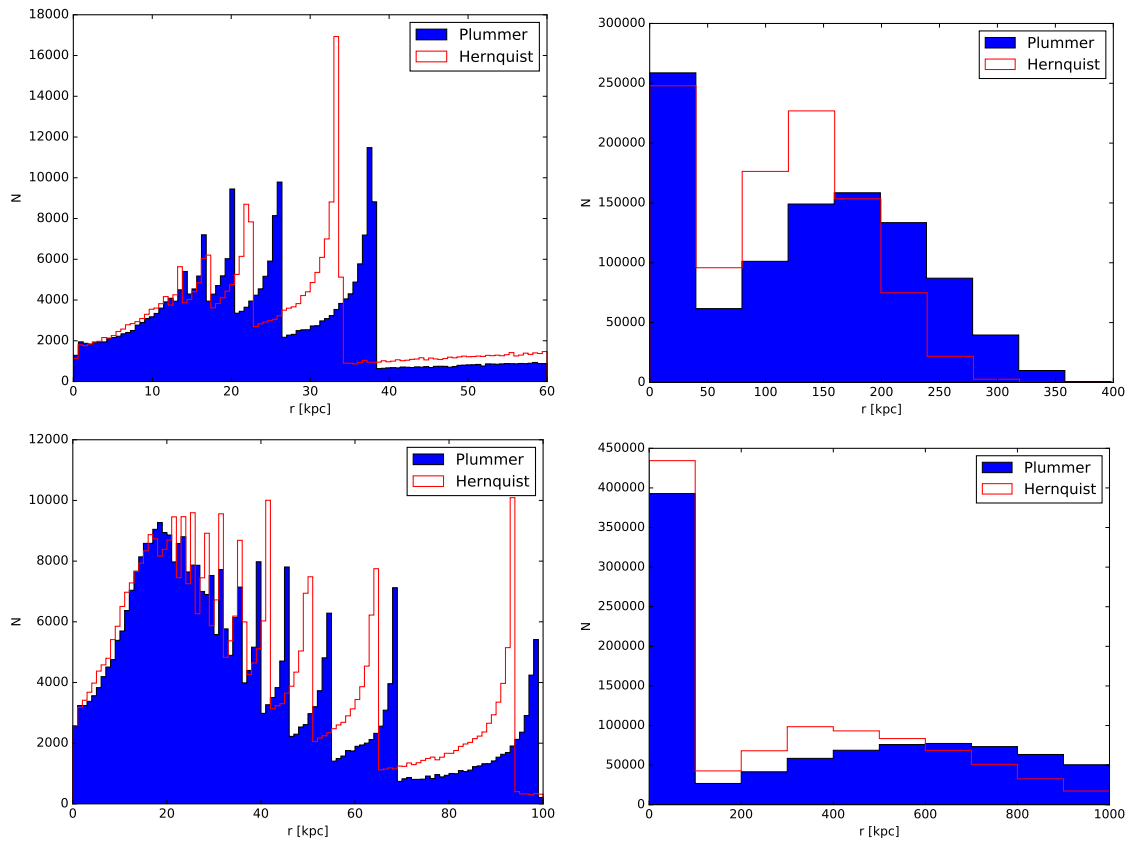Figure 3.7: Simulation of the merger with Hernquist potential shown in the phase space x - v_x.

Figure 3.8: Histograms of radial dependency of the test particles. Top two are at time $T = 1000$ Myr, bottom two at time $T = 3000$ Myr.
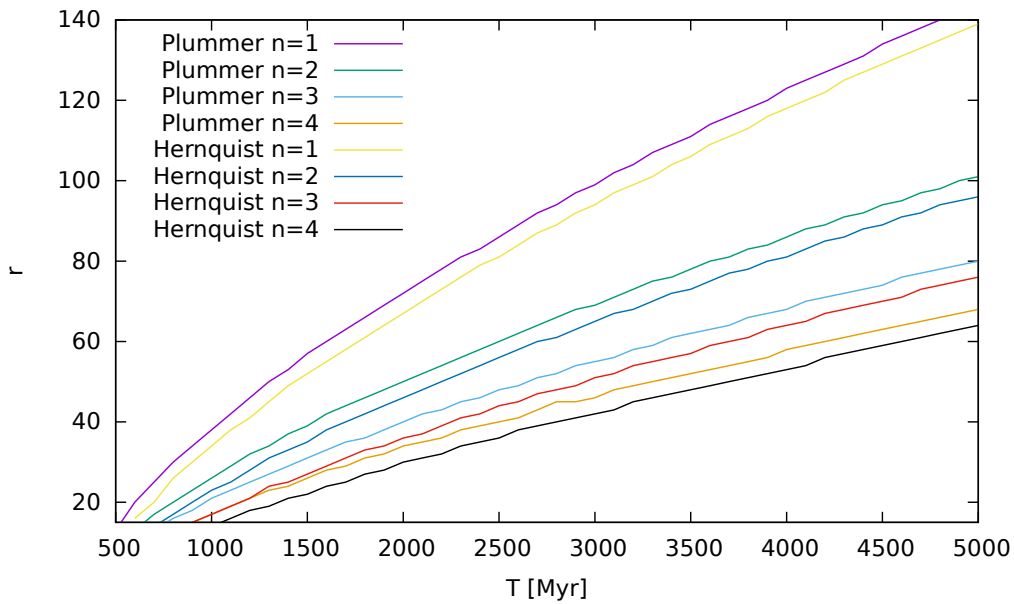

Figure 3.9: Time evolution of shell radii for the first four shells in both potentials.
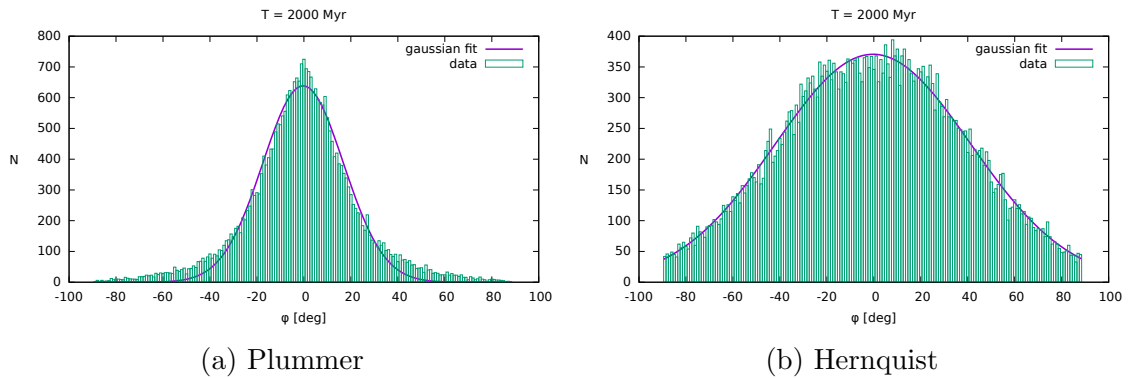
(a) Plummer
(b) Hernquist

Figure 3.10: Histograms showing angular distribution of stars in shell $n = 1$ for Plummer and Hernquist potential at time $T = 2000$ Myr.

$\Delta R_n = 0.1R$ for all the shell numbers n. Afterwards, histograms showing the angular distribution of particles are constructed. Since we want to quantitatively describe the angular width of the shell, we fit the histograms with Gaussian function

$$f(N) = A * \exp\left(\frac{-(N-B)^2}{\phi^2}\right),\qquad(3.2)$$

where A,B and ϕ are free parameters of the fit. The angular width is then determined by the ϕ parameter which represents full width at half maximum (FWHM). Histograms of the angular distribution are shown in Fig. 3.10 and for the graphs showing time dependency of $\phi(T)$ see Fig. 3.11. It is clearly shown that shells in Hernquist potential have much higher angular width, which confirms our assumption from the study of trajectory of one particle in both potentials. This fact suggests that the observations of angular width of shells could possibly be used to determine whether real galaxy potentials are cuspy or constant in core. Another important finding is that the angular width of shells slowly rises with time which is generally known fact called opening up of shells and the width also rises with shell number n, which can be seen in pictures showing particles in configuration space (Fig. 3.4 and Fig. 3.5).

3.2.1 Hernquist profile and time step size

During the analysis of the data from simulations with Hernquist potential, we had to deal with several difficulties concerning the time step of simulations. In the beginning, it was set to be $\Delta t = 0.5$ Myr. The data from these simulations showed double peak in angular distribution of stars in shells (see Fig. 3.12). This would be another significant difference between cuspy profile and that with a constant core. It could also confirm that some shell galaxies have cone around their major axis with lower star density in shells, something that is suggested in case of NGC 7600 (Fig. 1). This, however, proved to be just a consequence of a too big time step. Due to high force pull close to the center of the galaxy in case of Hernquist potential, some particles had their trajectories calculated badly. With the adjustment of a time step
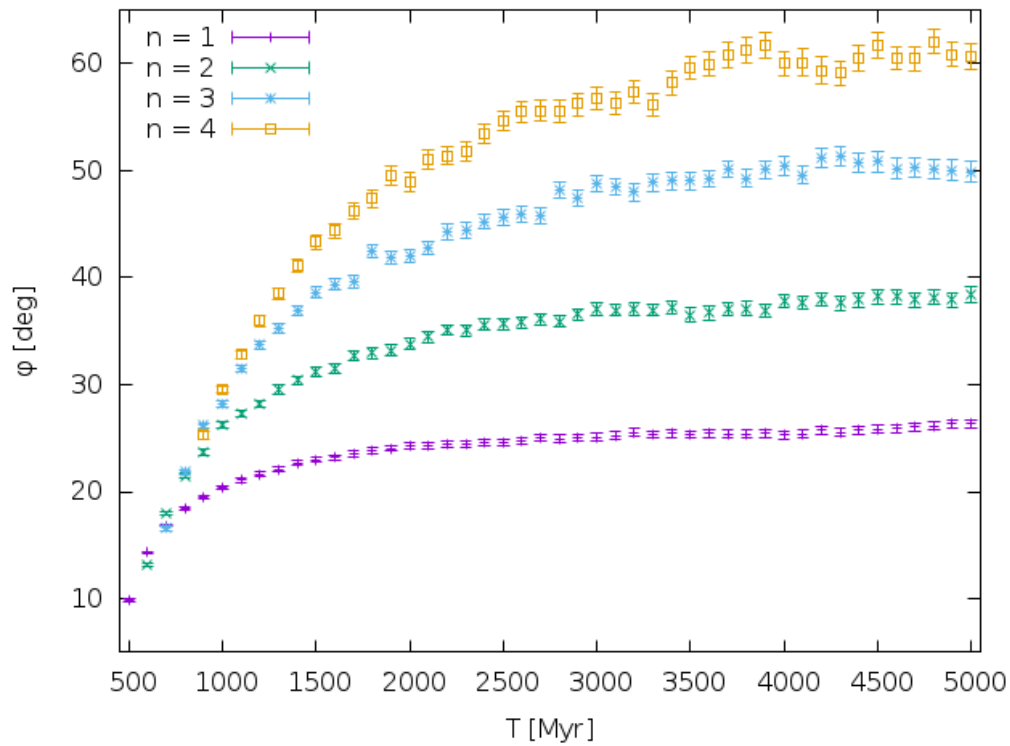
(a) Plummer
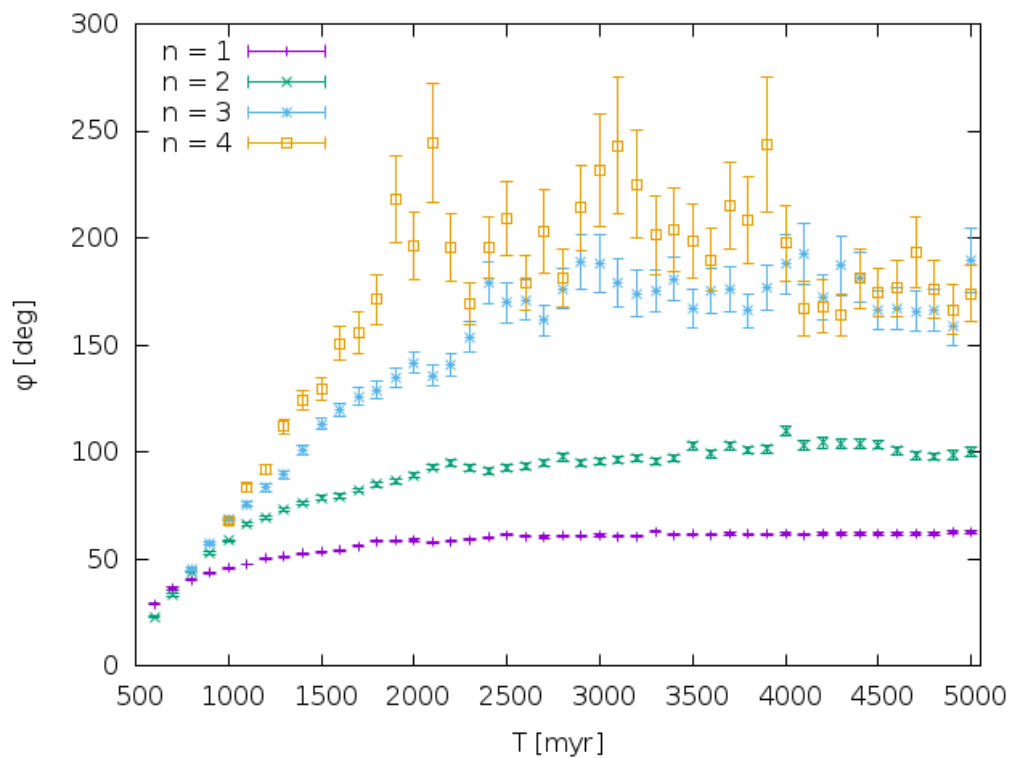
(b) Hernquist

Figure 3.11: Time evolution of the angular width of the first four shells for Plummer and Hernquist potential.
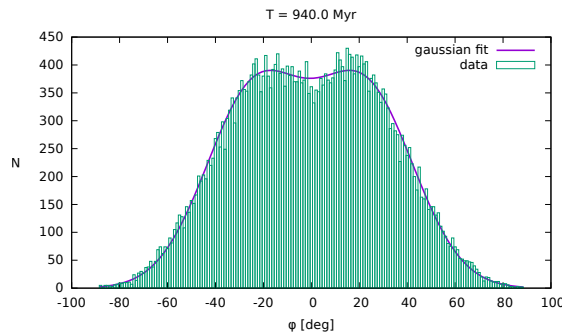
Figure 3.12: Histogram showing angular distribution of particles in Hernquist potential at time $T = 940$ Myr. Double peak is consequence of badly calculated trajectories of particles close to the center of the galaxy for too big time step $\Delta t = 0.5$ Myr.

$\Delta t = 0.1$ Myr, all of these double-peaked structures vanished as can be seen in Fig. 3.10.

3.3   The impact of different truncation radii

Both gravitational profiles used in our work are defined all the way to infinity, however, real galaxies don't spread that far away. In our simulations, this is achieved by truncating the galaxy at certain truncation radius R_{tr}. Particles generated outside of this radius or having velocity high enough to escape this radius are deleted and their positions and velocities are redrawn.

In this section we want to determine the effect of different truncation radii on radial and angular distribution of test particles. The reason behind this is that in general case, the gas and stellar component are not the same size (for our Galaxy, the gas component is approximately twice the size of stellar component) and this could affect the outcome of our simulations. In order to determine the effect of truncation radius, we generate two spheres containing 10^6 test particles for both potentials, one with $R_{tr} = 25$ kpc and second, twice the size, $R_{tr} = 50$ kpc. The outcome of these simulations is shown in Fig. 3.13 and Fig. 3.14.

From the graph showing radial distribution of shells we see, that positions of shells remain the same and they don't depend on truncation radius. Only shell intensities are affected. The angular width of shells does however change. We can clearly see that it is bigger for larger truncation radius. This fact is not a surprise since from the part 3.1, we know that the angular width of shells depends on positions of particle's apocenters and these are correlated with impact parameters. Spheres with larger truncation radius contain particles with higher impact parameters and that translates into their apocenters laying in higher angles measured from the x-axis. This fact should show up in our later simulations with gaseous shells.
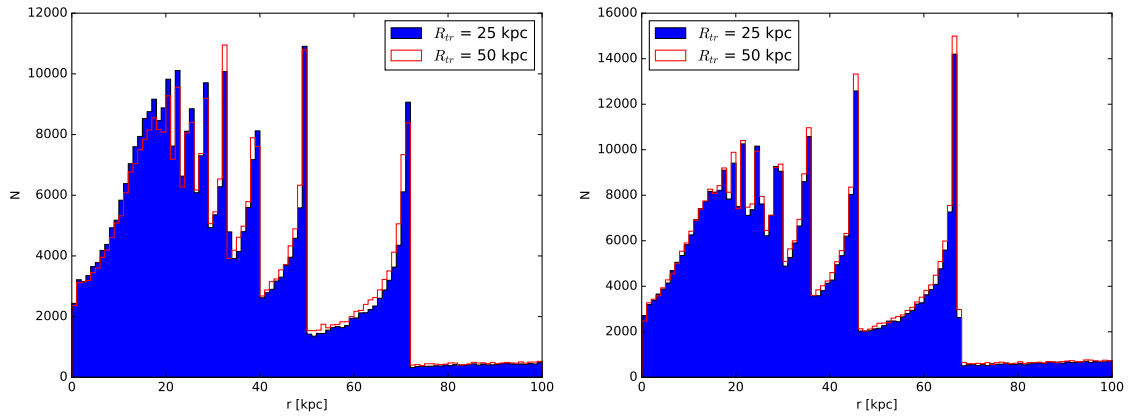
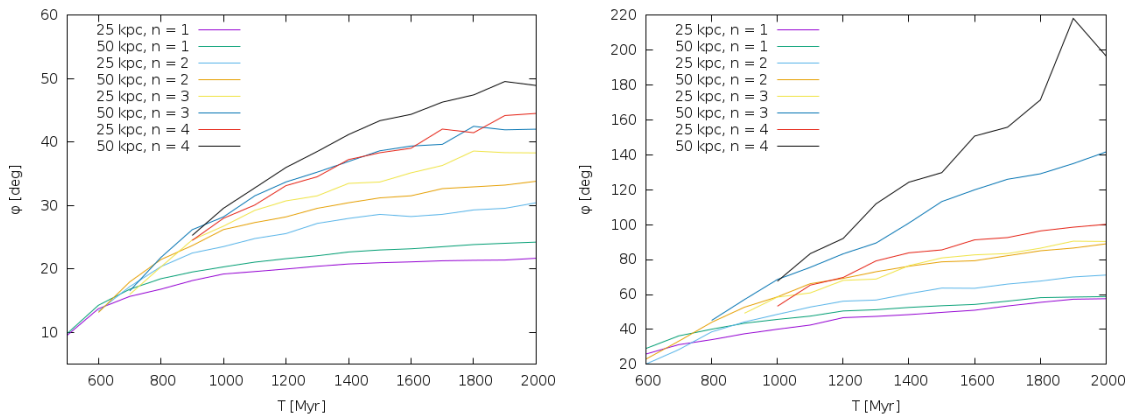Figure 3.13: Radial distribution of shells for two different R_{tr}.

Figure 3.14: Time development of the angular width of shells for two different R_{tr}.

Chapter 4

Simulations with hydrodynamics

Our goal in this section is to explore differences between stellar and gaseous shells. To achieve this, we simulated gas particles with the use of sticky-particles scheme, as described in part 2.4. Sticky-particles parameters were chosen $\beta_t = 1$, $\beta_r = 0.5$. In all the simulations, the secondary consists of 10000 sticky particles generated in truncated sphere and we chose two cloud radii $R_{\mathrm{cl}} = 10$ pc or 20 pc (typical sizes of molecular and atomic clouds). The truncation radius for gas is double the truncation radius for the stars. Reason for this is that in general, the size of gas and stellar components of a galaxy is not the same (in case of our Galaxy, the gas component is double the size of stellar component). In our simulations, we choose truncation radii $R_{\mathrm{tr,st}} = 2.5$ kpc for stellar component and $R_{\mathrm{tr,gas}} = 5$ kpc for gas component. The effect of different truncation radii was discussed in Part 3.3 and it has no effect on positions of shells, it only affects their angular width.

4.1 Hydrodynamic evolution of an isolated sphere

Our first goal was to simulate isolated sphere containing gas. This time evolution information is important to us, because the secondary is for the first several hundreds of Myr relatively far away from the primary and it evolves without primary's significant gravitational effect. A single isolated sphere was simulated consisting of 10000 sticky-particles of size $R_{\mathrm{cl}} = 10$ pc. The sphere is truncated at $R_{\mathrm{tr}} = 50$ kpc and it is let to evolve for 2000 Myr. Results in graphs are shown in Fig. 4.1. Only the graphs for Hernquist potential with $R_{\mathrm{cl}} = 10$ pc are shown, because graphs for Plummer potential were almost identical and hydrodynamic evolution of a Plummer sphere was examined in Zimandl (2015).

We can see that the Lagrange radius for 10% of mass is slowly shrinking while others are gradually increasing, most notably Lagrange radius for 90% of total mass. This suggests that the core of a galaxy is getting more dense with particles dissipating energy through collisions. This is confirmed by graph showing decrease of velocity dispersion for all Lagrange radii. Collisions do, however, also redistribute energy of particles which causes observed expansion of Lagrange radii for higher mass ratios. These effect get stronger with increasing size of gas particles R_{cl}.
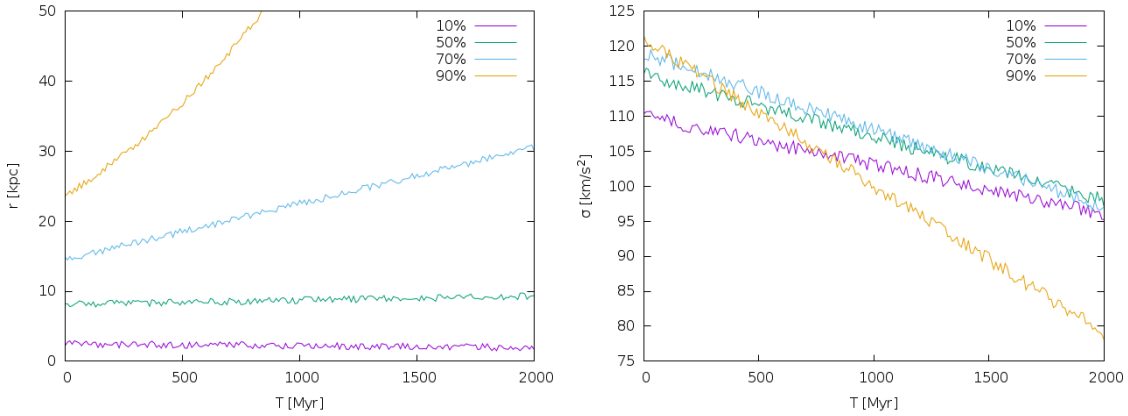
Figure 4.1: Graphs showing the time evolution of an isolated Hernquist sphere with sticky-particles of size $R_{cl} = 10$ pc. On the left is time evolution of Lagrange radii containing 10, 50, 70 and 90% of a total mass, on the right is time evolution of velocity dispersions for the same mass fractions.

4.2   Secondary galaxy with gas

The first merger simulations with gas were carried out for the system, where the secondary consist of 10000 sticky-particles, truncated at 5 kpc and 10000 test particles, representing stellar component, truncated at 2.5 kpc, the primary contains no particles. In our simulations, we used two cloud radii for the sticky-particles 10 pc and 20 pc. Histograms of radial distribution at time $T = 2000$ Myr are shown in Fig. 4.2 and Fig. 4.3.

The difference in position of the shells is almost nonexistent, the intensity of shells, however, differs and lowers with increase in size of the particles for both Plummer and Hernquist potential. In the histogram showing larger distances, we can also notice lower concentration of gas in the center of a galaxy (lesser that 100 kpc) and in distances higher than 400 kpc. Concentration of particle in distances 100-400 kpc is on the other hand higher than that of stars.

Zimandl (2015) provide this explanation: the decrease in number of gas particles in small and large radii means, that in the moment of secondary's decay, it contained less fast gas particles compared to stellar component, if the velocity is measured in secondary's frame of reference. The velocity in primary's frame of reference is calculated as particle velocity measured from secondary's frame of reference and velocity of the secondary from primary's frame of reference. Fast particles show up in histogram in large radii, if, in the moment of decay, they were moving roughly in direction of secondary's movement and if they moved the other way, their velocity after transformation is low and they oscillate near the center. Due to the fact that gas collisions reduce velocity dispersion in secondary (as discussed in Part 4.1) before the merger there is less fast particles which translates into lower concentrations in small and large radii.

Time evolution of the angular width of shells can be seen in Fig. 4.4. Due to the fact that the shells contain just a small number of sticky-particles, the fits of
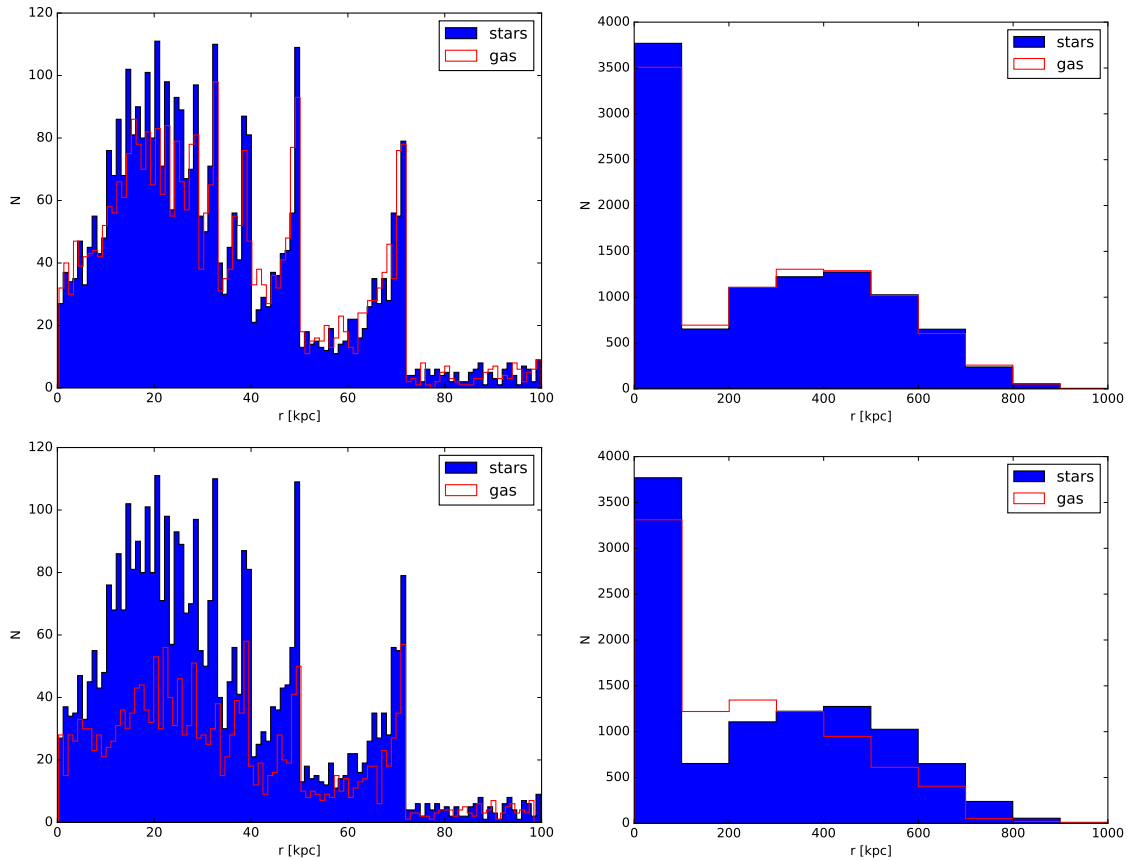
Figure 4.2: Histograms showing the radial dependency of the sticky-particles for Plummer potential. Top two are for $R_{cl} = 10$ pc, bottom two for $R_{cl} = 20$ pc.

Gaussian function are not exceptionally precise and should only be taken as a rough estimate. The general trend of gradual increase of the angular width is present and values for both R_{cl} tend to overlap with error bars, sometimes, however, there is an offset between the values. The widths of gaseous shells also roughly copy lines drawn for stellar shells and we don't observe any significant difference, as discussed in 3.3. Given the level of simplification used in our simulations, a low number of sticky-particles and subsequently a lot of noise, we should not draw any observable conclusions from this results.

4.3   Primary and secondary galaxy with gas

The last set of simulations was carried out for both galaxies containing gas particles. Secondary, again, consists of 10000 sticky-particles truncated at 5 kpc and 10000 test particles truncated at 2.5 kpc. This time, however, primary contains 20000 sticky-particles truncated at 50 kpc. Given the fact that most of the gas collisions happen near the center of galaxies, increased density of gas should result in more collisions. Histograms showing radial distribution of gas particles belonging to the secondary
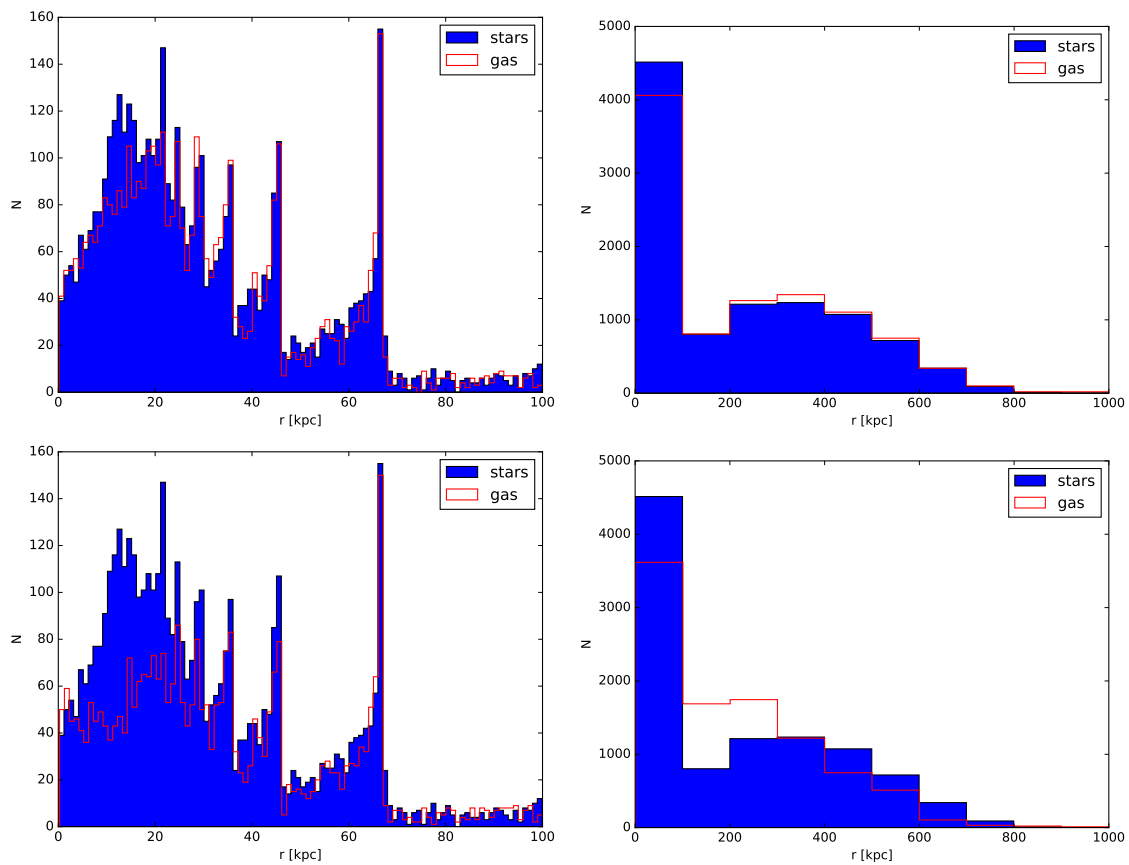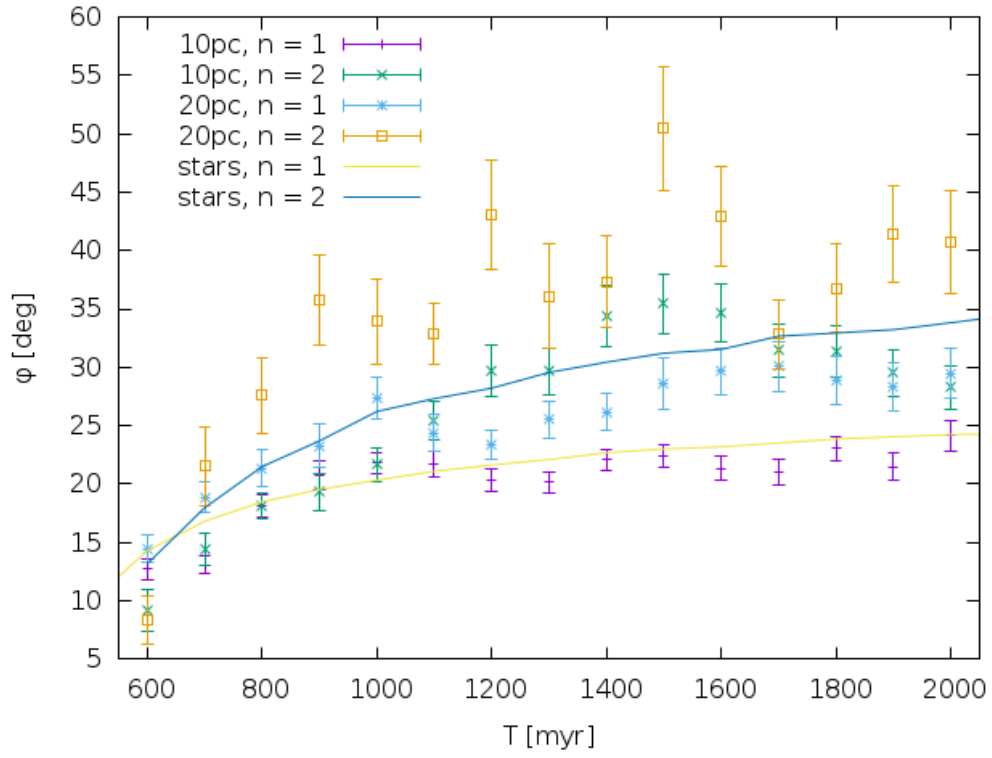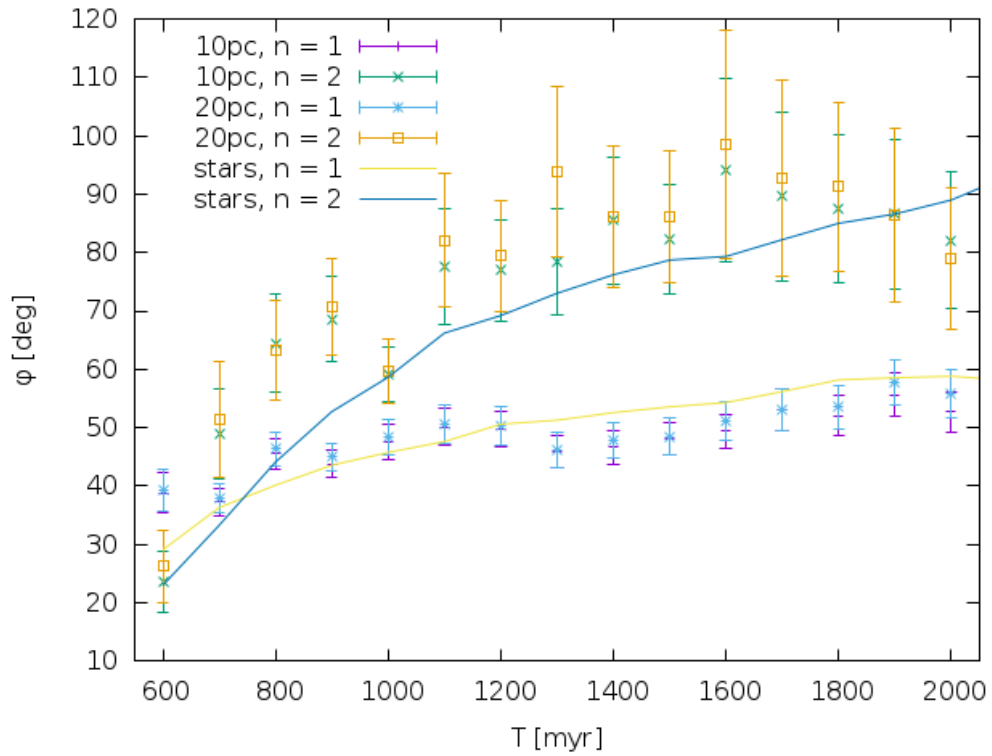
Figure 4.3: Histograms showing the radial dependency of the sticky-particles for Hernquist potential. Top two are for $R_{\mathrm{cl}} = 10$ pc, bottom two for $R_{\mathrm{cl}} = 20$ pc.

(a) Plummer

(b) Hernquist

Figure 4.4: Time evolution of the angular width of the first two shells for Plummer and Hernquist potential.
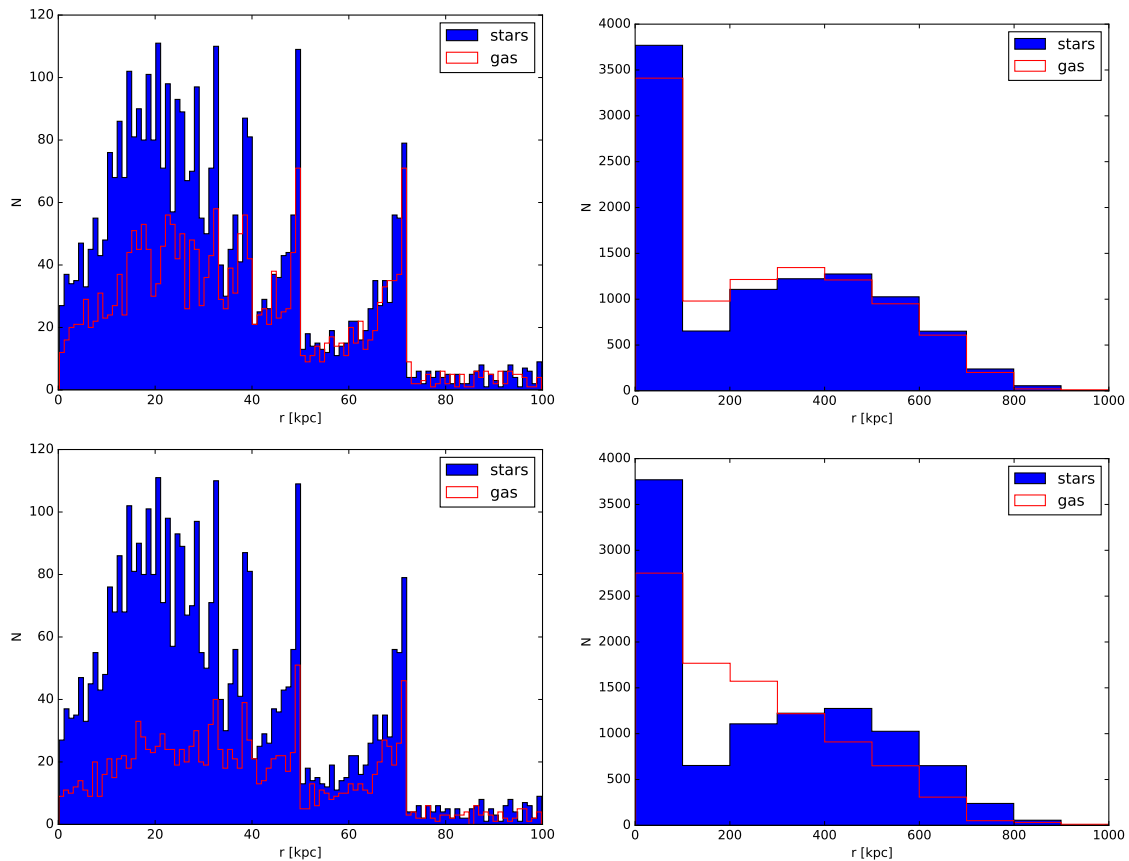
Figure 4.5: Histograms showing the radial dependency of the sticky-particles for Plummer potential in case when primary also contains gas. Top two are for $R_{cl} = 10$ pc, bottom two for $R_{cl} = 20$ pc.

before merger (gas particles of the primary are excluded from the graphs since they do not form shells) are shown in Fig. 4.5 and Fig. 4.6.

The positions of gaseous shells remain, again, virtually the same as the stellar shells. The intensity, on the other hand, differs significantly. Some inner shells even disappeared for $R_{cl} = 20$ pc in both profiles. This could be explained be gradual dissipation of energy in gas collisions, which are statistically more likely to happen to the fast oscillating particles forming inner shells. Significant increase in number of particles closer to the core is observed as well, which is also result of energy dissipation in sticky-particles collisions as well as energy redistribution in the secondary before the merger itself.

Time evolution of the angular width of shells can be seen in Fig. 4.7. Similarly to case with gas only in secondary (Fig. 4.4), the low number of particles and high noise in data dows not allow us to draw any observable conclusions.
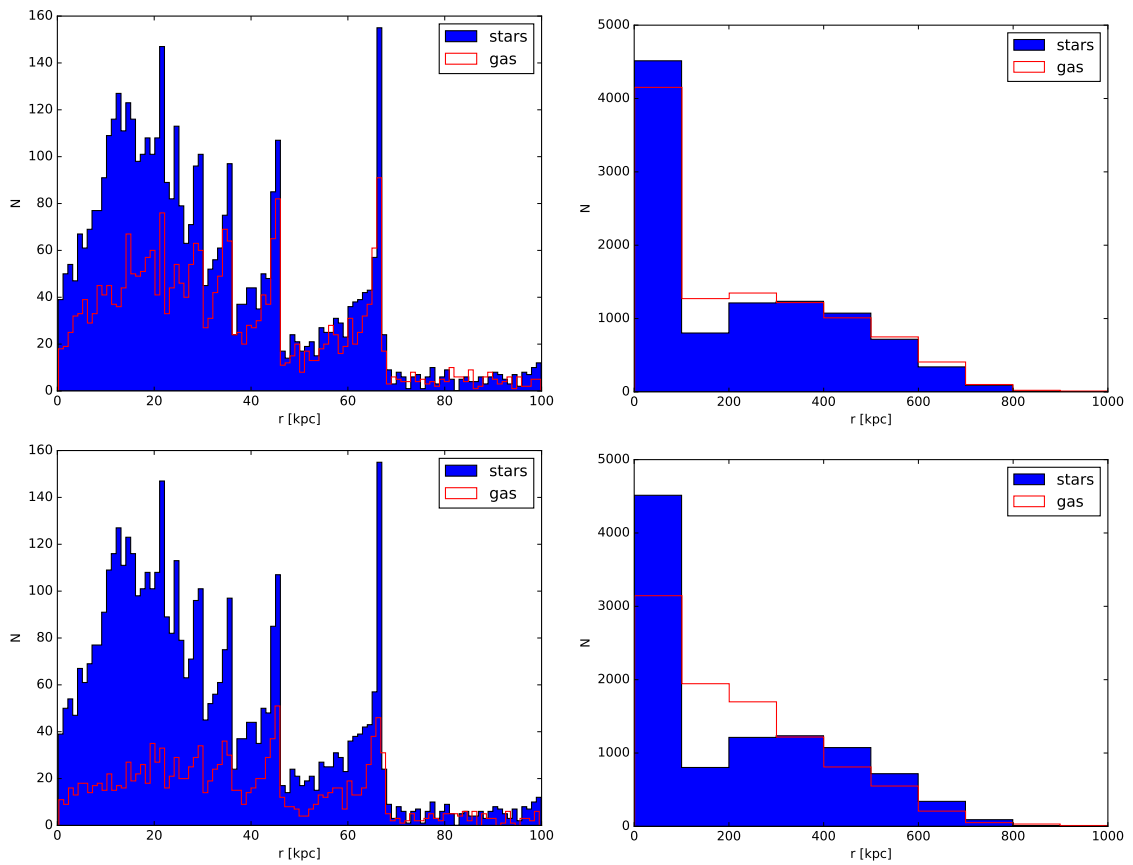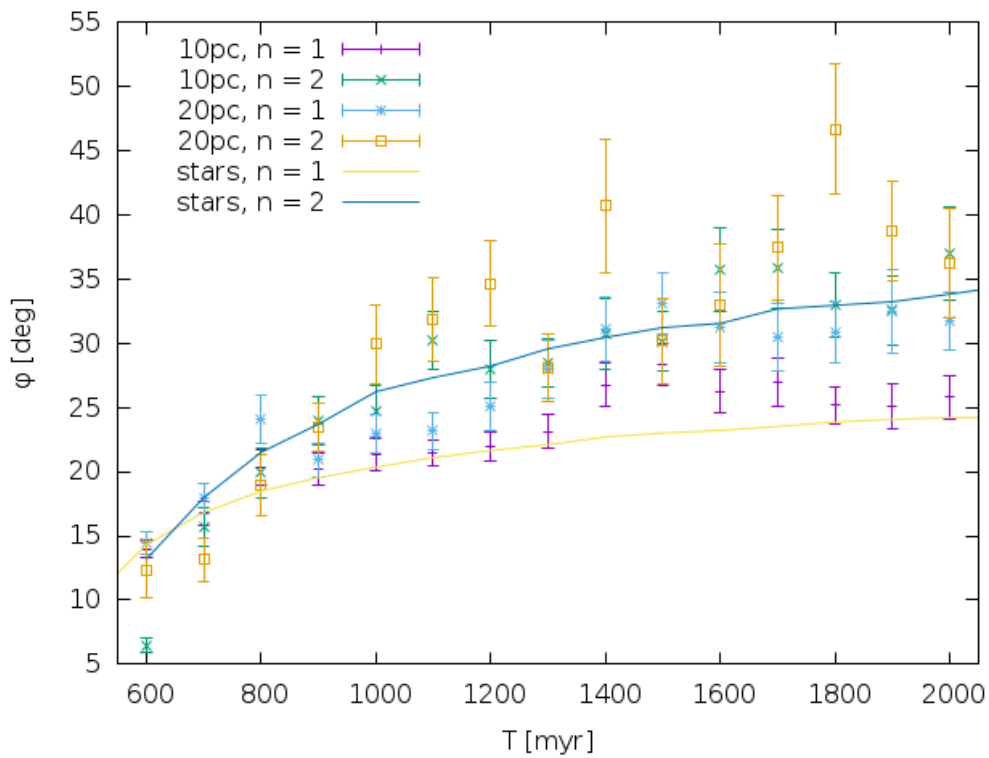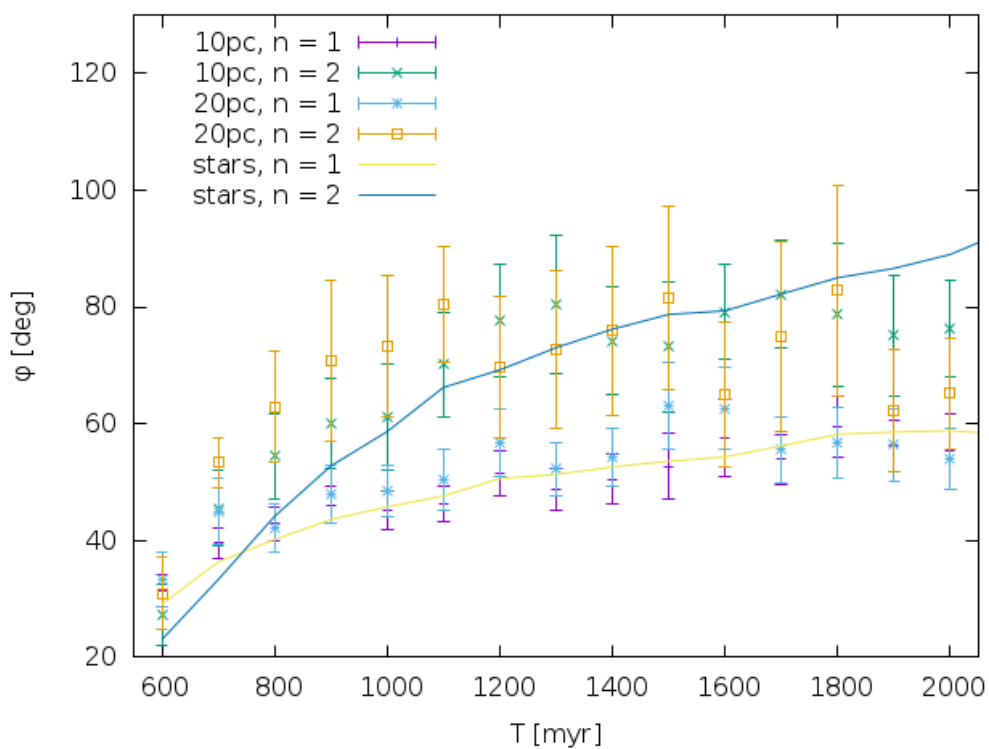
Figure 4.6: Histograms showing the radial dependency of the sticky-particles for Hernquist potential in case when primary also contains gas. Top two are for $R_{cl} = 10$ pc, bottom two for $R_{cl} = 20$ pc.

(a) Plummer

(b) Hernquist

Figure 4.7: Time evolution of the angular width of the first two shells for Plummer and Hernquist potential in case when primary also contains gas.

Chapter 5

Conclusion

In our work we used numerical simulations of radial encounters of high mass ratio spherical galaxies. Two analytical potentials were used - Plummer and Hernquist model. The stellar components of galaxies were simulated with test particles, that interact only gravitationally, the gaseous components were simulated using sticky-particles hydrodynamics. Our goal was to describe the differences between both potentials as well as between stellar and gaseous components of resulting shell galaxy. To achieve this, we used several simplifications.

To simulate galaxies, *spherically symmetrical analytical* models were used. A well known Plummer model was chosen because it has been used in past to simulate mergers and shell galaxies. Positions and velocities are easily generated from the distribution function. It is example of a model with a constant core in density. The second model we used is Hernquist model, which is example of a model with a cuspy profile with similar advantages as Plummer model. The use of analytical models does, however, bring some disadvantages as well. The decay of secondary had to be introduced artificially and lot of physical effect haven't been taken into account at all (e.g. gradual disruption of secondary, dynamical friction). From this point of view, the use of self-consistent simulations would have been better, because they would have these effect in them naturally. This would, however, demand far more computational resources.

Similarly to simplified potentials, we used *sticky-particles* hydrodynamics, that is easy to implement and does not have high demands on computers. On the other hand, it does introduce several free parameters β_r, β_t and R_{cl}, that are in reality difficult to determine. The cloud radii used in our simulations were 10 and 20 pc, which corresponds to typical sizes of molecular a atomic gas clouds. Smaller and larger clouds do exist in galaxies as well and their effect is not included in our simulations. The effect of non-discretely distributed gas was also not taken into account. The amount of gas particles was chosen to be 10000, which is pretty standard number for typical spiral galaxies, but not for small ellipticals, which was the case of secondary galaxy used. Young, high redshift galaxies did, however, contain these amounts of gas.

From the *simulations without gas*, we found out that shell galaxies can form after minor merger just as described in Quinn (1984). The differences between Plummer

and Hernquist profile were in positions of shells as well as their angular width, which was approximately twice as big for Hernquist profile, than for Plummer profile. This fact has to do with the density in center of both profiles and subsequently the force pull in their centers. Another effect related to this is that for higher *truncation radii*, we get slightly higher angular width of shells, but it does not affect the radial distribution of shells.

The simulations of *isolated spheres* showed that dissipation of energy because of collisions between gas particles does have more significant effect on the outcome of simulation, mainly in case of higher cloud radii. Center of the galaxy is getting more dense, which results in more collisions and redistribution of energy. This showed in graphs as a drop in number of particles close to the core and further than 400 kpc and rise in numbers of particles at radii 100-400 kpc.

The simulations with *gas in secondary* showed us, that using sticky-particles scheme, gaseous shells do originate. Hydrodynamics do not have huge impact in radial distribution of shells, only their intensity is affected. The angular width of gaseous shells showed roughly the same time evolution as that of stellar shells, but we were unable to draw any observable conclusions. The most important effect was the redistribution of energy in secondary before the merger.

Results taken from simulations with *gas in secondary and primary* showed, that gas in primary can have significant effect on the outcome of simulations, mainly for gas particles with high cloud radius. It leads into the core of the galaxy getting denser much faster and thus some of the inner shells vanished completely. As for the angular width of shells, the results are again not conclusive due to low amount of gas particles in shells.

In general, we can say that the hydrodynamics has almost no effect on the radial distribution of shells and it doesn't seem like it has any significant effect on the angular width of shells either. The only observable conclusion from our work is definite differences between Plummer and Hernquist potential, which could help us determine shape of real galactic potentials.

Bibliography

H. Arp. Atlas of Peculiar Galaxies. *ApJS*, 14:1, Nov. 1966. doi: 10.1086/190147.

G. Canalizo, N. Bennert, B. Jungwiert, A. Stockton, F. Schweizer, M. Lacy, and C. Peng. Spectacular Shells in the Host Galaxy of the QSO MC2 1635+119. *ApJ*, 669:801–809, Nov. 2007. doi: 10.1086/521721.

D. Carter, D. A. Allen, and D. F. Malin. Nature of the shells of NGC1344. *Nature*, 295:126–128, Jan. 1982. doi: 10.1038/295126a0.

V. Charmandaris, F. Combes, and J. M. van der Hulst. First detection of molecular gas in the shells of CenA. *AA*, 356:L1–L4, Apr. 2000.

M. Coleman, G. S. da Costa, D. Martínez-Delgado, and J. Bland-Hawthorn. Substructure in the Fornax dSph Galaxy: A Possible Merger Remnant. In F. Prada, D. Martinez Delgado, and T. J. Mahoney, editors, *Satellites and Tidal Streams*, volume 327 of *Astronomical Society of the Pacific Conference Series*, page 173, Dec. 2004.

F. Combes and V. Charmandaris. Formation of Gaseous Shells. In F. Combes, G. A. Mamon, and V. Charmandaris, editors, *Dynamics of Galaxies: from the Early Universe to the Present*, volume 197 of *Astronomical Society of the Pacific Conference Series*, page 339, 2000.

C. Dupraz and F. Combes. Shells around galaxies - Testing the mass distribution and the 3-D shape of ellipticals. *AA*, 166:53–74, Sept. 1986.

I. Ebrová, B. Jungwiert, G. Canalizo, N. Bennert, and L. Jílková. Shell Galaxies: Dynamical Friction, Gradual Satellite Decay and Merger Dating. In B. Smith, J. Higdon, S. Higdon, and N. Bastian, editors, *Galaxy Wars: Stellar Populations and Star Formation in Interacting Galaxies*, volume 423 of *Astronomical Society of the Pacific Conference Series*, page 236, June 2010.

A. C. Fabian, P. E. J. Nulsen, and G. C. Stewart. Star formation in a galactic wind. *Nature*, 287:613, Oct. 1980. doi: 10.1038/287613a0.

M. A. Fardal, P. Guhathakurta, A. Babul, and A. W. McConnachie. Investigating the Andromeda stream - III. A young shell system in M31. *MNRAS*, 380:15–32, Sept. 2007. doi: 10.1111/j.1365-2966.2007.11929.x.

M. A. Fardal, A. Babul, P. Guhathakurta, K. M. Gilbert, and C. Dodge. Was the Andromeda Stream Produced by a Disk Galaxy? *ApJl*, 682:L33–L36, July 2008. doi: 10.1086/590386.

B. P. Fort, J.-L. Prieur, D. Carter, S. J. Meatheringham, and L. Vigroux. Surface photometry of shell galaxies. *ApJ*, 306:110–121, July 1986. doi: 10.1086/164324.

A. Helmi, J. F. Navarro, A. Meza, M. Steinmetz, and V. R. Eke. On the Nature of the Ringlike Structure in the Outer Galactic Disk. *ApJl*, 592:L25–L28, July 2003. doi: 10.1086/377364.

L. Hernquist. An analytical model for spherical galaxies and bulges. *ApJ*, 356: 359–364, June 1990. doi: 10.1086/168845.

L. Hernquist and P. J. Quinn. Formation of shell galaxies. I - Spherical potentials. *ApJ*, 331:682–698, Aug. 1988. doi: 10.1086/166592.

L. Hernquist and P. J. Quinn. Formation of shell galaxies. II - Nonspherical potentials. *ApJ*, 342:1–16, July 1989. doi: 10.1086/167571.

E. P. Hubble. *Realm of the Nebulae.* 1936.

M. Kojima and M. Noguchi. Sinking Satellite Disk Galaxies. I. Shell Formation Preceded by Cessation of Star Formation. *ApJ*, 481:132–156, May 1997.

W. Kundt and M. Krause. The nature of the IGM. *AA*, 142:150–156, Jan. 1985.

D. F. Malin and D. Carter. A catalog of elliptical galaxies with shells. *ApJ*, 274: 534–540, Nov. 1983. doi: 10.1086/161467.

W. D. Pence. Spectrophotometry of shell galaxies. *ApJ*, 310:597–604, Nov. 1986. doi: 10.1086/164712.

H. C. Plummer. On the problem of distribution in globular star clusters. *MNRAS*, 71:460–470, Mar. 1911.

J.-L. Prieur. *Status of shell galaxies.*, pages 72–83. 1990.

P. J. Quinn. On the formation and dynamics of shells around elliptical galaxies. *ApJ*, 279:596–609, Apr. 1984. doi: 10.1086/161924.

D. Schiminovich, J. H. van Gorkom, J. M. van der Hulst, and S. Kasow. Discovery of Neutral Hydrogen Associated with the Diffuse Shells of NGC 5128 (Centaurus A). *ApJl*, 423:L101, Mar. 1994. doi: 10.1086/187246.

D. Schiminovich, J. H. van Gorkom, J. M. van der Hulst, and D. F. Malin. Neutral hydrogen associated with shells and other fine structure in NGC 2865: A dynamically young elliptical? *ApJl*, 444:L77–L80, May 1995. doi: 10.1086/187864.

D. Schiminovich, J. van Gorkom, T. van der Hulst, T. Oosterloo, and A. Wilkinson. Imaging and Kinematics of Neutral Hydrogen in and around "Shell Galaxies". In M. Arnaboldi, G. S. Da Costa, and P. Saha, editors, *The Nature of Elliptical Galaxies; 2nd Stromlo Symposium*, volume 116 of *Astronomical Society of the Pacific Conference Series*, page 362, 1997.

D. Schiminovich, J. H. van Gorkom, and J. M. van der Hulst. Extended Neutral Hydrogen in the Aligned Shell Galaxies Arp 230 and MCG -5-7-1: Formation of Disks in Merging Galaxies? *AJ*, 145:34, Feb. 2013. doi: 10.1088/0004-6256/145/2/34.

F. Schweizer. An optical study of the giant radio galaxy NGC 1316 /Fornax A/. *ApJ*, 237:303–318, Apr. 1980. doi: 10.1086/157870.

F. Schweizer and P. Seitzer. Ripples in disk galaxies. *ApJ*, 328:88–92, May 1988. doi: 10.1086/166270.

G. Sikkema, D. Carter, R. F. Peletier, M. Balcells, C. Del Burgo, and E. A. Valentijn. HST/ACS observations of shell galaxies: inner shells, shell colours and dust. *AA*, 467:1011–1024, June 2007. doi: 10.1051/0004-6361:20077078.

R. C. Thomson and A. E. Wright. A Weak Interaction Model for Shell Galaxies. *MNRAS*, 247:122, Nov. 1990.

A. J. Turnbull, T. J. Bridges, and D. Carter. Imaging of the shell galaxies NGC 474 and 7600, and implications for their formation. *MNRAS*, 307:967–976, Aug. 1999. doi: 10.1046/j.1365-8711.1999.02724.x.

M. L. Weil and L. Hernquist. Segregation of gas and stars in shell galaxies. *ApJ*, 405:142–152, Mar. 1993. doi: 10.1086/172347.

A. Wilkinson, W. B. Sparks, D. Carter, and D. A. Malin. Two Colour CCD Photometry of Malin / Carter Shell Galaxies. In P. T. de Zeeuw, editor, *Structure and Dynamics of Elliptical Galaxies*, volume 127 of *IAU Symposium*, page 465, 1987.

R. E. Williams and W. A. Christiansen. Blast wave formation of the extended stellar shells surrounding elliptical galaxies. *ApJ*, 291:80–87, Apr. 1985. doi: 10.1086/163043.

M. Zimandl. Slupkové galaxie - hydrodynamické simulace typu "sticky-particles". Master thesis, Karlova univerzita, Matematicko-fyzikální fakulta, Praha, 2015.